© 2017. Published by The Company of Biologists Ltd | Development (2017) 144, 1906-1917 doi:10.1242/dev.147512

RESEARCH ARTICLE

Embryonic cholecystitis and defective gallbladder contraction in the *Sox17*-haploinsufficient mouse model of biliary atresia

Hiroki Higashiyama[1,*], Aisa Ozawa[1,*], Hiroyuki Sumitomo[1,*], Mami Uemura[1,2,*], Ko Fujino[1], Hitomi Igarashi[1], Kenya Imaimatsu[1], Naoki Tsunekawa[1], Yoshikazu Hirate[2], Masamichi Kurohmaru[1], Yukio Saijoh[3], Masami Kanai-Azuma[2] and Yoshiakira Kanai[1,‡]

ABSTRACT

The gallbladder excretes cytotoxic bile acids into the duodenum through the cystic duct and common bile duct system. *Sox17* haploinsufficiency causes biliary atresia-like phenotypes and hepatitis in late organogenesis mouse embryos, but the molecular and cellular mechanisms underlying this remain unclear. In this study, transcriptomic analyses revealed the early onset of cholecystitis in *Sox17*$^{+/-}$ embryos, together with the appearance of ectopic cystic duct-like epithelia in their gallbladders. The embryonic hepatitis showed positive correlations with the severity of cholecystitis in individual *Sox17*$^{+/-}$ embryos. Embryonic hepatitis could be induced by conditional deletion of *Sox17* in the primordial gallbladder epithelia but not in fetal liver hepatoblasts. The *Sox17*$^{+/-}$ gallbladder also showed a drastic reduction in sonic hedgehog expression, leading to aberrant smooth muscle formation and defective contraction of the fetal gallbladder. The defective gallbladder contraction positively correlated with the severity of embryonic hepatitis in *Sox17*$^{+/-}$ embryos, suggesting a potential contribution of embryonic cholecystitis and fetal gallbladder contraction in the early pathogenesis of congenital biliary atresia.

KEY WORDS: Gallbladder, Biliary atresia, *Sox17*, *Shh*

INTRODUCTION

The gallbladder is a flexible organ of the biliary tract that regulates bile storage and discharge by the contractile movement of its smooth muscles. Malformation of the gallbladder and bile ducts can cause disease, including cholesterol gallstones, chronic inflammation and biliary atresia (reviewed by Portincasa et al., 2004, 2008; Asai et al., 2015). Congenital biliary atresia is a rare condition in newborn infants (Kohsaka et al., 2002; Mieli-Vergani and Vergani, 2009) that causes inflammation in the bile ducts and liver due to the blockage of bile flow (cholestasis). It is usually characterized by an aberrant gallbladder of reduced length, with irregular walls and indistinct mucosal lining, that appears to be closely associated with neonatal cholestasis associated with severe inflammation of the intrahepatic ducts (Desmet, 1992; Mack and Sokol, 2005; Mieli-Vergani and Vergani, 2009).

The etiology of human biliary atresia remains unclear. It is speculated to be caused by either environmental factors, such as viral infections or toxin exposure in genetically susceptible individuals, or by developmental errors during the specification and morphogenesis of bile duct epithelia (reviewed by Mack and Sokol, 2005; Mieli-Vergani and Vergani, 2009; Nakamura and Tanoue, 2013; Davenport, 2016). Whether a result of internal or external factors, epithelial defects and/or injury of the extrahepatic bile ducts may be associated with the onset of human biliary atresia by the neonatal stage (Mack and Sokol, 2005; Davenport, 2016).

The extrahepatic biliary structures (gallbladder, cystic duct, hepatic ducts and common bile duct) originate from the biliary primordium (Spence et al., 2009; Uemura et al., 2010, 2013), which expresses SRY-box 17 (*Sox17*), a core regulator of endoderm determination in mice and humans (Tam et al., 2003). Formation of the intrahepatic duct is regulated cooperatively by *Sox9* and *Sox4* (Poncy et al., 2015), albeit that their roles in the extrahepatic duct remain unclear. In a previous study (Uemura et al., 2013), perinatal lethality was observed in ∼90% of *Sox17* heterozygous (*Sox17*$^{+/-}$) mice and the embryos displayed defective development of the gallbladder including defective bile duct epithelial wall and a biliary atresia-like phenotype (an abnormal accumulation of luminal decidual cells in the bile duct), together with severe embryonic hepatitis after the first biliary excretion into the fetal duodenum at ∼16.5 days post coitum (dpc). This timing of biliary atresia-like symptoms in mouse embryos is consistent with the hypothesis of early onset of biliary atresia in human fetuses (Tan et al., 1994; reviewed by Davenport, 2016). In human fetuses, bile acid synthesis occurs during the early organogenesis stages, during which bile starts to be excreted into the intestine near the end of the first trimester (Nakagawa and Setchell, 1990 and references therein). Furthermore, recent studies of naturally occurring outbreaks of sheep biliary atresia revealed that biliatresone, a causative toxin for biliary atresia, reduces *Sox17* expression levels in the bile duct epithelia, and that silencing *Sox17* mimics the effects of biliatresone on the bile duct epithelia (Lorent et al., 2015; Waisbourd-Zinman et al., 2016). Together with the extensive anatomical similarity of the extrahepatic biliary tracts and the associated blood vessels, nerves and smooth muscles between mice and humans (Higashiyama et al., 2016), the *Sox17*$^{+/-}$ mouse embryo provides a useful experimental model with which to study the initial pathogenesis of biliary atresia.

In this study, we demonstrate the early onset of cholecystitis in the cystic duct-like gallbladder of *Sox17*$^{+/-}$ mouse embryos, in which the reduction in sonic hedgehog (*Shh*) expression leads to defective contraction of the smooth muscles.

[1]Department of Veterinary Anatomy, The University of Tokyo, Yayoi 1-1-1, Bunkyo-ku, Tokyo 113-8657, Japan. [2]Center for Experimental Animals, Tokyo Medical and Dental University, Yushima 1-5-45, Bunkyo-ku, Tokyo 113-8510, Japan. [3]Department of Neurobiology and Anatomy, The University of Utah, Salt Lake City, UT 84132-3401, USA.
*These authors contributed equally to this work and are joint first authors

‡Author for correspondence (aykanai@mail.ecc.u-tokyo.ac.jp)

H.H., 0000-0003-1324-8139; A.O., 0000-0002-0506-5909; H.S., 0000-0003-0916-7846; M.U., 0000-0003-0036-3103; Y.K., 0000-0003-2116-7806

Received 27 November 2016; Accepted 12 April 2017

Development (2017) 144, 1906-1917 doi:10.1242/dev.147512

RESULTS

SOX9-positive cystic duct-like epithelia in the *Sox17*$^{+/-}$ primordial gallbladder

In wild-type embryos, the fetal gallbladder forms a pseudostratified columnar epithelium with epithelial folds by 17.5 dpc, while the cystic duct consists of a single-layered cuboidal epithelium with few epithelial folds throughout the fetal stages (Fig. 1A). The *Sox17*$^{+/-}$ gallbladder shows severe hypotrophy and a single-layered cuboidal epithelium with few epithelial folds (Fig. 1A) (see also Uemura et al., 2013), similar in appearance to the cystic duct epithelia of wild-type embryos at the same stage (17.5 dpc). This is consistent with morphometric data showing a significant reduction in epithelial height, cavity and/or epithelial area of the *Sox17*$^{+/-}$ gallbladder, such that these values are similar to those of wild-type cystic ducts (Fig. 1B).

SOX17 is highly expressed in the developing gallbladder and cystic duct epithelia. It is enriched in the distal region of the developing gallbladder epithelium. This is in contrast to the restricted distribution of SOX9-positive epithelial cells to the proximal region of the cystic duct (Fig. 1C; Fig. S1), thus showing a mostly non-overlapping pattern between distal SOX17-positive and proximal SOX9-positive epithelial cells in the gallbladder of wild-type embryos. In the *Sox17*$^{+/-}$ gallbladder, the SOX9-positive domain expands into the distal region in the gallbladder (Fig. 1D), despite the reduced proliferation in the proximal cystic duct domain of the *Sox17*$^{+/-}$ versus wild-type gallbladder (Fig. S2). qPCR analysis confirms that *Sox9* expression is significantly increased in *Sox17*$^{+/-}$ gallbladder compared with wild type at 15.5 dpc (Fig. 1E). Considering our previous observation of hypoplasia and deciduation in the *Sox17*$^{+/-}$ gallbladder epithelia (Uemura et al., 2013), these data suggest that the gallbladder epithelial cells might be replaced with the ectopic SOX9-positive cystic duct-like epithelial cells. In addition, such elevated expression of *Sox9* in the *Sox17*$^{+/-}$ gallbladder correlates with the subsequent expression of *Sox4*, which can act redundantly with *Sox9* in intrahepatic duct formation (Poncy et al., 2015) (Fig. S3).

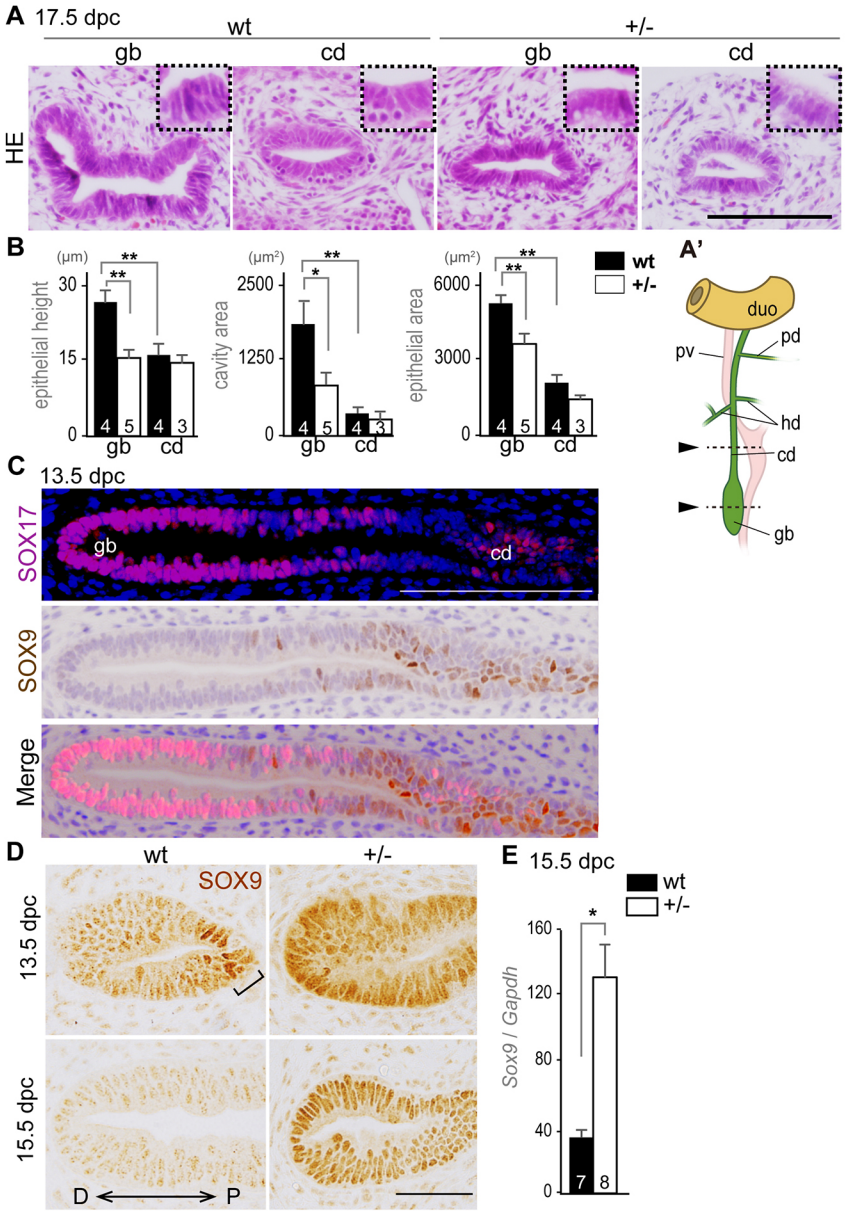

Fig. 1. *Sox17*$^{+/-}$ gallbladder epithelium exhibits cystic duct-like phenotypes. (A) Transverse sections [Hematoxylin and Eosin (HE) staining] of the gallbladder and cystic duct from wild-type (wt) and *Sox17*$^{+/-}$ mouse embryos at 17.5 dpc. The levels of the sections are indicated in A′ (arrowheads). Insets show high magnification images of the epithelium. (B) Quantitative analyses show a significant reduction in epithelial height and epithelial/cavity areas of the gallbladder in *Sox17*$^{+/-}$ embryos at 17.5 dpc. **P*<0.05, ***P*<0.01, ANOVA followed by Tukey's test. (C) Anti-SOX17 and anti-SOX9 double immunohistochemistry in the primordial gallbladder and cystic duct regions of the wild-type embryo at 13.5 dpc. (D) *Sox17*$^{+/-}$ embryos display ectopic SOX9-positive cells in the distal edge of the gallbladder at 13.5 and 15.5 dpc. Bracket indicates the SOX9-positive domain. (E) qPCR analysis indicates a significant increase in *Sox9* mRNA in the *Sox17*$^{+/-}$ gallbladder at 15.5 dpc. **P*<0.05, Student's *t*-test. In B and E, sample number is indicated within each bar. cd, cystic duct; duo, duodenum; gb, gallbladder; hd, hepatic duct; pd, pancreatic duct; pv, portal vein; D, distal; P, proximal. Scale bars: 100 μm.

Development (2017) 144, 1906-1917 doi:10.1242/dev.147512

Onset of cholecystitis in *Sox17*$^{+/-}$ gallbladder during fetal stages

To examine the transcriptomic changes in the *Sox17*$^{+/-}$ gallbladder, microarray analyses were conducted using gallbladder (distal) and cystic duct (proximal) segments of the *Sox17*$^{+/-}$ and wild-type gallbladder primordia at 15.5 dpc, before the first secretion of bile fluid from the fetal liver (Uemura et al., 2013) (Fig. 2A,B). The transcriptomic analysis identified 279 upregulated and 501 downregulated genes in *Sox17*$^{+/-}$ gallbladder compared with wild-type littermates at 15.5 dpc (n=4; Table S1). Gene set enrichment analysis (GSEA) confirmed *Sox9* among the top 50 enriched/upregulated genes in the *Sox17*$^{+/-}$ gallbladder (Fig. S4). Moreover, these data were compared with those of gallbladder-specific or cystic duct-specific genes from the same littermates [5361 or 4886 genes (n=2) expressed at higher or lower levels, respectively, in the gallbladder segment compared with the cystic duct segment of wild-type embryos]. Of the downregulated genes in the *Sox17*$^{+/-}$ gallbladder, 207/279 (74.4%) overlap with the gallbladder-specific genes that we identified (Fig. 2A, Table 1). Furthermore, of the upregulated genes, 221/501 (44.1%) overlap with the cystic duct-specific gene list (Fig. 2B, Table 1). This is consistent with data showing the appearance of SOX9-positive cystic duct-like epithelia in the *Sox17*$^{+/-}$ gallbladder during the late fetal stages (Fig. 1).

GSEA showed an enrichment of genes in the category ‘definitive hemopoiesis’ (Fig. S4). Gene ontology (GO) analysis confirmed that the 280 upregulated genes, other than the 221 cystic duct-specific genes, are involved in ‘myeloid cell differentiation’ (*Klf1*, *Tal1*, *Epb42*, *Ahsp*, *Prdx3*, *Psen2* and *Trim10*) (Fig. 2B), suggesting the enrichment of immature hematopoietic cells (e.g. inflammation) in the fetal gallbladder region even at 15.5 dpc. Key marker genes of several hepatobiliary and digestive tract disorders were also upregulated in this dataset, including olfactomedin 4 (*Olfm4*) (Liu et al., 2010; Gersemann et al., 2012), ATP-binding cassette, subfamily B4 (*Abcb4*) (Fickert et al., 2004; Esten Nakken et al., 2007; Baghdasaryan et al., 2011; Gordo-Gilart et al., 2015) and polycystic kidney and hepatic disease 1 (*Pkhd1*) (Nakamura et al., 2010; Hartley et al., 2011). We therefore examined the expression

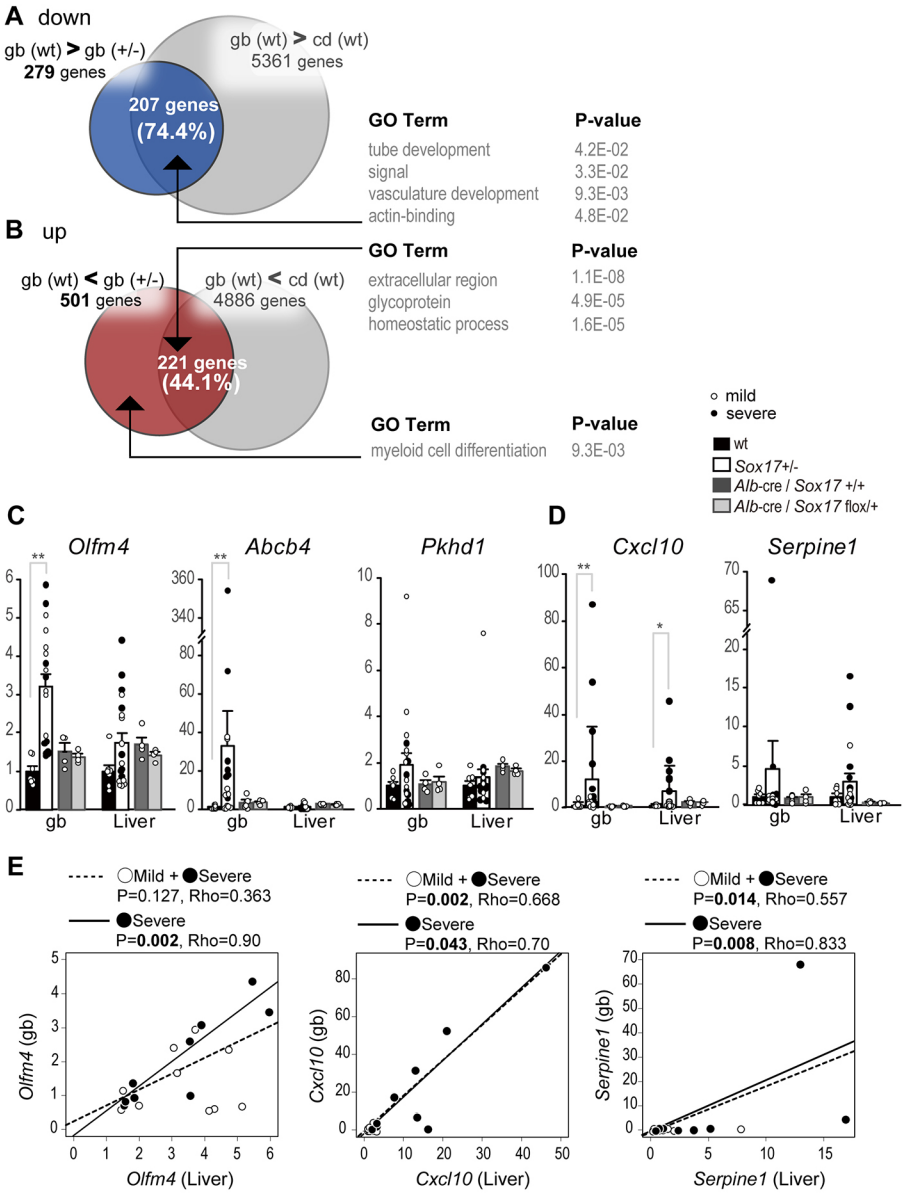

Fig. 2. Global expression profiles and cholecystitis of fetal *Sox17*$^{+/-}$ gallbladders. (A,B) Microarray analysis identifies 279 downregulated genes (blue circle in A) and 501 upregulated genes (red circle in B) in the *Sox17*$^{+/-}$ gallbladder at 15.5 dpc, as compared with gallbladder from wild-type (wt) littermates. Among these downregulated or upregulated genes, 207 (74.4%) or 221 (44.1%) were shared with the 5361 gallbladder-specific or 4886 cystic duct (cd)-specific genes, respectively, in wild-type embryos at the same stage. (C,D) qPCR analyses showing the upregulated profiles of the biliary disease marker genes *Olfm4*, *Abcb4* and *Pkhd1* (C) and the inflammatory marker genes *Cxcl10* and *Serpine1* (D) in *Sox17*$^{+/-}$ gallbladder at 17.5 dpc. The *y*-axis is fold change in expression level of each gallbladder or liver sample relative to those of the wild type (mean value set to 1). Each solid or open circle indicates a sample from an embryo with (severe phenotype) or without (mild phenotype) gross anatomical hepatic lesions, respectively. Bar charts show the average mean values of all (severe and mild) samples. The expression level of each marker gene in the *Alb*-cre/*Sox17*$^{+/+}$ and *Alb*-cre/*Sox17*$^{flox/+}$ embryos at the same stage is also shown. **P*<0.05, ***P*<0.01, Mann-Whitney U-test. (E) Spearman rank correlation analysis of the association between gallbladder (*y*-axis) and liver (*x*-axis) phenotypes for the indicated genes in *Sox17*$^{+/-}$ embryos at 17.5 dpc. Both axes represent fold change in expression relative to wild-type littermates (mean value set to 1). In *Sox17*$^{+/-}$ embryos, significant correlations between the two tissues were detected in both the severe phenotype and all (mild and severe phenotype) samples for *Cxcl10* and *Serpine1* mRNA levels, and in only the severe phenotype samples for *Olfm4*.

Development (2017) 144, 1906-1917 doi:10.1242/dev.147512

Table 1. Top 15 of the 207 downregulated (gallbladder-specific) or the 221 upregulated (cystic duct-specific) genes in *Sox17*$^{+/-}$ gallbladders at 15.5 dpc

Description	Gene	Fold change									
Downregulated genes		**gb (+/–)<gb (wt)** (reduced levels)						**cd (wt)<gb (wt)** (gb-specific genes)			
Cbp/p300-interacting transactivator with Glu/Asp-rich carboxy-terminal domain 1	*Cited1*	**–9.1**	(–10.3,	–6.3,	–12.7,	–10.1)		**–5.8**	(–5.9,	–7.6)	
Sonic hedgehog	*Shh*	**–9.0**	(–9.4,	–7.0,	–13.4,	–8.7)		**–11.3**	(–16.1,	–6.4)	
Maltase-glucoamylase	*Mgam*	**–5.6**	(–11.0,	–6.2,	–5.0,	–3.2)		**–2.9**	(–1.4,	–4.6)	
Pro-melanin-concentrating hormone	*Pmch*	**–4.7**	(–3.5,	–6.8,	–4.5,	–4.7)		**–5.2**	(–5.0,	–4.8)	
Cytochrome P450, family 2, subfamily f, polypeptide 2	*Cyp2f2*	**–4.1**	(–3.2,	–4.9,	–3.4,	–3.0)		**–3.9**	(–1.5,	–5.6)	
S100 calcium-binding protein G	*S100g*	**–4.0**	(–4.4,	–6.5,	–3.7,	–2.8)		**–3.5**	(–3.2,	–2.1)	
Hedgehog-interacting protein	*Hhip*	**–3.5**	(–3.4,	–2.7,	–3.8,	–4.8)		**–3.5**	(–4.0,	–3.7)	
Rho GTPase activating protein 36	*1100001E04Rik* (*Arhgap36*)	**–3.4**	(–3.3,	–5.3,	–2.4,	–2.6)		**–6.7**	(–2.8,	–4.9)	
Janus kinase and microtubule interacting protein 2	*Jakmip2*	**–3.4**	(–7.5,	–3.5,	–2.8	–2.5)		**–1.8**	(–2.5,	2.1)	
Cytochrome c oxidase, subunit VIIa 1	*Cox7a1*	**–3.1**	(–2.4,	–3.1,	–4.0,	–3.7)		**–3.1**	(–2.9,	–3.8)	
Solute carrier family 14 (urea transporter), member 1	*Slc14a1*	**–3.1**	(–2.9,	–3.0,	–2.6,	–4.4)		**–2.3**	(–1.3,	–3.2)	
ADAM-like, decysin 1	*Adamdec1*	**–3.1**	(–2.9,	–4.3,	–2.4,	–4.1)		**–3.8**	(–3.3,	–4.7)	
SRY-box 17	*Sox17*	**–3.1**	(–2.4,	–2.8,	–3.9,	–3.5)		**–3.4**	(–3.4,	–2.8)	
Cholecystokinin A receptor	*Cckar*	**–3.0**	(–1.7,	–2.6,	–4.9,	–3.3)		**–6.6**	(–12.1,	–3.7)	
Cytochrome P450, family 4, subfamily x, polypeptide 1	*Cyp4x1*	**–2.9**	(–3.1,	–4.8,	–1.7,	–2.8)		**–2.6**	(–1.5,	–1.6)	
Upregulated genes		**gb (+/–)>gb (wt)** (elevated levels)						**cd (wt)>gb (wt)** (cd-specific genes)			
Extracellular proteinase inhibitor	*Expi* (*Wfdc18*)	**4.2**	(4.5,	3.3,	2.8,	6.2)		**2.3**	(1.5,	5.2)	
RIKEN cDNAB130021B11 gene	*B130021B11Rik*	**3.5**	(2.4,	2.0,	1.5,	2.2)		**3.6**	(2.2,	2.3)	
Polycystic kidney and hepatic disease 1	*Pkhd1*	**3.3**	(2.8,	1.0,	1.6,	5.7)		**1.6**	(2.1,	–1.4)	
Carboxylesterase 3	*Ces3*	**3.1**	(4.6,	2.0,	2.1,	3.7)		**5.1**	(9.3,	4.1)	
Claudin 8	*Cldn8*	**3.0**	(4.7,	1.7,	2.2,	4.3)		**2.1**	(2.6,	3.1)	
Apolipoprotein A-II	*Apoa2*	**2.9**	(1.3,	–1.0,	10.5,	2.4)		**11.9**	(44.7,	8.2)	
DNA segment, Chr 4, Brigham&Women's Genetics 0951 expressed, mRNA	*D4Bwg0951e* (*Lurap1l*)	**2.8**	(3.3,	2.8,	1.9,	3.5)		**1.7**	(1.9,	1.3)	
Insulin-like growth factor binding protein 1	*Igfbp1*	**2.8**	(4.0,	1.1,	4.9,	3.0)		**4.6**	(8.9,	9.0)	
TAO kinase 3	*Taok3*	**2.7**	(4.5,	–1.2,	1.4,	1.5)		**3.2**	(2.1,	–2.0)	
Transcription elongation factor A (SII)-like 7	*RP23-105O4.2* (*Tceal7*)	**2.7**	(21.3,	1.6,	1.4,	–1.1)		**2.0**	(1.3,	1.9)	
Solute carrier family 34 (sodium phosphate), member 2	*Slc34a2*	**2.6**	(2.7,	2.0,	2.8,	4.9)		**4.4**	(3.6,	6.3)	
Lectin, galactose binding, soluble 3	*Lgals3*	**2.6**	(1.5,	1.2,	14.4,	2.1)		**2.8**	(22.4,	3.2)	
Pregnancy zone protein	*Pzp*	**2.5**	(1.6,	–1.3,	9.9,	3.1)		**12.2**	(43.2,	15.9)	
Reelin	*Reln*	**2.4**	(2.6,	1.8,	1.7,	4.4)		**5.0**	(4.4,	6.7)	
Golgi apparatus protein 1	*Glg1*	**2.4**	(2.4,	–1.1,	3.1,	1.2)		**1.8**	(1.7,	–1.3)	

Microarray expression analyses were performed using the presumptive gallbladder (gb, distal) and cystic duct (cd, proximal) segments of the primordial gallbladder of *Sox17*$^{+/-}$ (+/–) and wild-type (wt) embryos at 15.5 dpc. Fold changes that are in bold are from quadruplicate or duplicate microarray data generated by AltAnalyze; the numbers in parentheses indicate the fold changes in each individual. Each value in parenthesis represents one relative value of two hybridization signals, i.e. A/a, B/b, C/c and D/d ('+/– versus wt' or 'cd versus gb') of four array experiments. Mean value in bold is (A+B+C+D)/(a+b+c+d) for each probe generated by AltAnalyze. Gallbladder-specific or cystic duct-specific genes were defined as exhibiting a difference of at least 1.5-fold between the gallbladder and cystic duct regions, respectively, of wild-type embryos at 15.5 dpc.

levels of these three disease markers, in addition to two inflammatory markers, namely *Cxcl10* (Leonhardt et al., 2006) and *Serpine1* (Bessho et al., 2014), in both gallbladder and liver samples isolated from *Sox17*$^{+/-}$ embryos with or without hepatic lesions (severe or mild phenotype group) at 17.5 dpc (Fig. 2C,D; Fig. S5A).

qPCR analysis showed a significant increase in the expression of *Olfm4*, *Abcb4* and *Cxcl10* in the *Sox17*$^{+/-}$ gallbladder compared with the wild-type gallbladder (Fig. 2C,D, left two bars in gb), in addition to high expression levels of both *Olfm4* and *Cxcl10* in the severely affected livers (Fig. 2C,D, solid circles in 'liver'). *Serpine1* expression appeared to be higher, albeit not significantly, in both the gallbladder and liver of some severe phenotype *Sox17*$^{+/-}$ embryos. Among these four genes, we found significant positive correlations in the increased expression levels of *Olfm4* (only severe samples), *Cxcl10* and *Serpine1* (both severe and mild samples) between gallbladder and liver samples (Spearman test; Fig. 2E; see also Fig. S5B), suggesting a positive correlation in phenotypic severity between the gallbladder (i.e. cholecystitis) and intrahepatic regions (i.e. hepatitis) in *Sox17*$^{+/-}$ embryos. Interestingly, *Abcb4* expression was increased only in gallbladder and not liver tissues (Fig. 2C; Fig. S5A), suggesting a potentially useful marker specific for extrahepatic cholestasis (Schaap et al., 2009).

Pkhd1, which encodes the ciliary protein fibrocystin, was upregulated in several mild phenotype samples (without any gross anatomical hepatic lesions) (Fig. 2C; Fig. S5A). In *Sox17*$^{+/-}$ gallbladders, we found a positive correlation between *Pkhd1* and *Olfm4* expression levels independent of gross anatomical hepatic lesions, in addition to the negative correlation between *Pkhd1* and *Abcb4* expression levels (Fig. S5C).

In addition, qPCR analysis of several fetal myeloid cell markers, namely *Tal1* (Kelliher et al., 1996), *Klf1* (McConnell and Yang, 2010) and *Prdx3* (Park et al., 2016), revealed a tendency for an increase in their expression levels in the *Sox17*$^{+/-}$ gallbladder region, together with a positive correlation among these three genes (Fig. S6A,B). Moreover, immunohistochemical analysis revealed that Gr1 (LY6G)-positive or F4/80 (ADGRE1)-positive spherical

Development (2017) 144, 1906-1917 doi:10.1242/dev.147512

myeloid-like cells appeared to be enriched in the surrounding mesenchymal region of the *Sox17*$^{+/-}$ gallbladder, albeit with no direct infiltration into the epithelial layers of the *Sox17*$^{+/-}$ gallbladder (Fig. S6C).

Fetal liver phenotypes induced by conditional deletion of *Sox17* in liver hepatoblasts or primordial gallbladder epithelia

Sox17 is expressed not only in the primordial gallbladder, but also in a population of hepatoblast progenitor cells at early somite stages (Okada et al., 2012). To specify the contribution of reduced *Sox17* activity in the liver or gallbladder in the onset of embryonic hepatitis, we examined the liver phenotypes of *Sox17*^{flox} embryos with a conditional deletion of *Sox17* using albumin (*Alb*)-cre and *Pdx1*-cre mice. In contrast to *Alb*-cre-dependent recombination of the *ROSA*^{mTmG} allele in liver hepatoblasts (Fig. 3A), *Pdx1*-cre was able to induce recombination in approximately half of the fetal gallbladder and cystic duct epithelia by 17.5 dpc (Fig. 3A), in addition to its efficient deletion of *Sox17* in the pancreas and duodenum, with both tissues showing no detectable *Sox17* expression at these stages (Spence et al., 2009; Uemura et al., 2010).

First we examined the liver and gallbladder phenotypes of *Alb*-cre/*Sox17*$^{flox/+}$ embryos, and these showed no developmental defects in liver and gallbladder development (data not shown). qPCR analysis confirmed no elevated expression of the inflammatory marker genes in gallbladder or liver of *Alb*-cre/*Sox17*$^{flox/+}$ embryos at 17.5 dpc (Fig. 2C,D, two righthand bars in each group), suggesting no appreciable link to hepatitis of the reduced *Sox17* expression in the liver hepatoblasts. The *Alb*-cre/*Sox17*$^{flox/flox}$ embryos also showed normal liver and gallbladder phenotypes (Fig. 3B).

By contrast, *Pdx1*-cre/*Sox17*$^{flox/flox}$ embryos showed severe gross anatomical hepatic lesions in some embryos (4/55 embryos; Fig. 3B), together with elevated *Cxcl10* and *Serpine1* expression in the affected livers (Fig. 3C). Moreover, the *Pdx1*-cre/*Sox17*$^{flox/flox}$ embryos showed varying degrees of shortening of the gallbladder and cystic duct (Fig. 3D), with hepatitis observed in fetuses with normal (type I, 3/34 embryos in Fig. 3D) and mild (type II, 1/10 embryos) phenotypes, but no hepatitis in individuals with a complete lack of the gallbladder (type III, 0/11 embryos). Moreover, histopathological and qPCR analyses confirmed that *Pdx1*-cre/*Sox17*$^{flox/flox}$ embryos show biliary atresia-like phenotypes similar to those of *Sox17*$^{+/-}$ embryos, such as epithelial deciduation, bile duct stenosis/atresia and reduced *Shh* expression (Fig. S7) (Uemura et al., 2013; this study). These data suggest that the hepatitis in *Sox17*$^{+/-}$ embryos is caused by reduced *Sox17* activity in the primordial gallbladder, and is not associated with the liver hepatoblasts.

Several *Shh*-related genes are downregulated in the *Sox17*$^{+/-}$ gallbladder

Among the 207 downregulated genes in the *Sox17*$^{+/-}$ gallbladder at 15.5 dpc (Fig. 2A, Table 1; Fig. S4), we focused on the altered expression of *Shh* and of the *Shh*-responsive gene *Hhip*. Whole-mount *in situ* hybridization analysis of wild-type embryos at 11.5-13.5 dpc revealed that *Shh*, as well as *Sox17*, was expressed in the

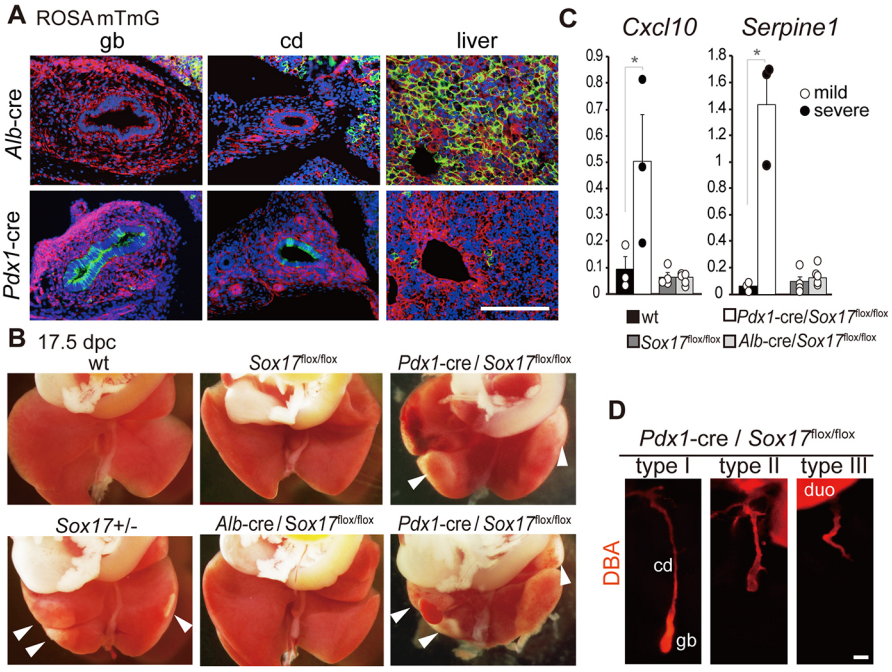

Fig. 3. Embryonic hepatitis can be induced by conditional *Sox17* deletion in primordial gallbladder but not in liver hepatoblasts. (A) Fluorescent images of gallbladder (gb), cystic duct (cd) and liver at 17.5 dpc, showing a liver-specific or gallbladder-specific fluorescent switch (from red to green) in *Alb*-cre/*ROSA*^{mTmG} or *Pdx1*-cre/*ROSA*^{mTmG} embryos, respectively. The *Pdx1*-cre/*ROSA*^{mTmG} embryo shows recombination in approximately half of the gallbladder and cystic duct epithelia by 17.5 dpc. (B) Caudal views of the fetal liver at 17.5 dpc. Peripheral inflammation of the liver lobules (arrowheads) is evident in two *Pdx1*-cre/*Sox17*$^{flox/flox}$ embryos (top, type I; bottom, type II; see D), but not in the *Alb*-cre/*Sox17*$^{flox/flox}$ embryo. Normal healthy livers (from wild-type and *Sox17*$^{flox/flox}$ embryos) and a typical defective liver (*Sox17*$^{+/-}$ embryo) are also shown. (C) qPCR analyses showing upregulation of the inflammatory marker genes *Cxcl10* and *Serpine1* in three *Pdx1*-cre/*Sox17*$^{flox/flox}$ livers with appreciable gross anatomical lesions (solid circles). Expression data of wild type, *Sox17*$^{flox/flox}$ and *Alb*-cre/*Sox17*$^{flox/flox}$ are also shown. *P<0.05, Mann-Whitney U-test. (D) DBA staining showing phenotypic variation of the gallbladder and cystic duct in individual *Pdx1*-cre/*Sox17*$^{flox/flox}$ embryos: type I (normal length of the gallbladder and cystic duct, 34/55 embryos), type II (half-length, 10/55) and type III (lack of the gallbladder and cystic duct, 11/55). duo, duodenum. Scale bars: 200 µm.

Development (2017) 144, 1906-1917 doi:10.1242/dev.147512

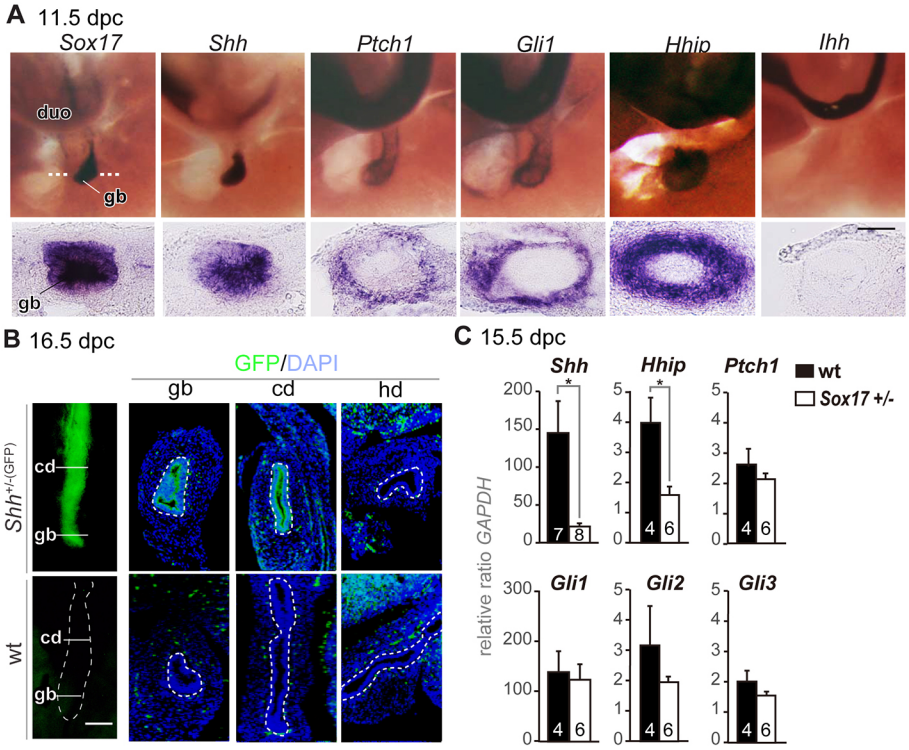

Fig. 4. Expression profiles of *Shh* and its downstream genes in the developing gallbladder. (A) Whole-mount *in situ* hybridization (top) and section (bottom; at the level of the gallbladder, indicated by the dotted line) images, showing the expression of *Sox17*, *Shh* and *Shh*-related genes in wild-type embryos at 11.5 dpc. *Sox17* and *Shh* are highly expressed in the gallbladder epithelia, in contrast to the mesenchymal enrichment for *Ptch1*, *Gli1* and *Hhip*. (B) Whole-mount GFP fluorescence (left) and anti-GFP-stained sections (three right images) of $Shh^{+/-(GFP)}$ and wild-type embryos at 16.5 dpc, showing GFP/*Shh*-positive epithelial signals in the gallbladder and cystic duct, but not in the hepatic ducts. Ducts are outlined. (C) qPCR analyses showing expression levels of *Shh* and related genes in $Sox17^{+/-}$ embryos. **P*<0.05, Student's *t*-test. Sample number is indicated within each bar. cd, cystic duct; duo, duodenum; gb, gallbladder; hd, hepatic duct. Scale bars: 100 µm.

epithelium of the distal portion of gallbladder (Fig. 4A). This is in contrast to the lack of positive signals for *Ihh*, the paralog of *Shh*, in the gallbladder (Fig. 4A). *Ptch1*, *Gli1* and *Hhip* were highly expressed in mesenchymal tissues adjacent to the gallbladder epithelium. Analysis using the $Shh^{+/-(GFP)}$ line confirmed expression of *Shh* in the bile duct epithelium of both the gallbladder and cystic duct, but not in the hepatic ducts, at 16.5 dpc (Fig. 4B). These expression data suggest a potential epithelial-mesenchymal interaction for SHH signaling in developing gallbladders of mid-to-late organogenesis stage embryos.

Next, we examined the expression levels of *Shh* and related genes using qPCR. Both *Shh* and *Hhip* were significantly downregulated in the $Sox17^{+/-}$ gallbladder (P<0.05), as compared with the wild-type gallbladder at 15.5 dpc (Fig. 4C). The expression levels of *Gli1*, *Gli3* and *Ptch1* were not affected, whereas *Gli2* expression tended to be reduced, albeit not significantly, in the $Sox17^{+/-}$ gallbladders (Fig. 4C).

Full activity of either *Sox17* or *Shh* is required for proper formation of smooth muscle layers in the developing gallbladder

The liver and gallbladder phenotypes were examined in wild-type, $Shh^{+/-}$ and $Shh^{-/-}$ embryos at 14.5-17.5 dpc. The gross anatomical and histopathological analyses appeared normal in the $Shh^{+/-}$ livers, which were similar to those of wild-type littermates. $Shh^{-/-}$ embryos, by contrast, were headless and exhibited severe growth retardation in the liver, albeit without any sign of hepatic inflammation (Fig. S8). Whole-mount DBA (*Dolichos biflorus* agglutinin) staining for the bile duct revealed a shortened gallbladder and cystic duct, accompanied by a reduction in size of the whole liver in $Shh^{-/-}$ embryos (14.5 dpc, Fig. 5A). However, in contrast to the shortened gallbladder length, transverse sectioning analysis revealed that the $Shh^{-/-}$ gallbladder epithelium was histologically normal, and SOX17-positive cells were present and indistinguishable from those in wild type (Fig. 5B). The proportion of PCNA-positive or Ki67-positive cells among total cells showed no appreciable differences in the gallbladder epithelia among wild-type, $Shh^{+/-}$ and $Shh^{-/-}$ embryos at 14.5 dpc (Fig. 5B,C; Fig. S9). Cumulatively, these data suggest that there are no appreciable defects in epithelial proliferation of $Shh^{-/-}$ gallbladder primordia, which is in sharp contrast to the hypoplasia of the $Sox17^{+/-}$ gallbladder epithelium at the same stages (Uemura et al., 2013).

Next, we examined the gallbladder phenotypes of $Sox17^{+/-}$; $Shh^{+/-}$ double-heterozygous embryos at 14.5-17.5 dpc (Fig. 5D-H). Histopathological analyses revealed no appreciable changes in epithelial morphology or anti-SOX9 or anti-SOX17 immunostaining intensity between $Sox17^{+/-}$ and $Sox17^{+/-}$;$Shh^{+/-}$ gallbladders, except for one severe sample showing luminal cell debris in the presumptive gallbladder region (1/4 $Sox17^{+/-}$;$Shh^{+/-}$ embryos; Fig. 5D, right; Fig. S10). Quantitative data also confirmed that there were no significant alterations in epithelial height between $Shh^{+/-}$ and $Shh^{+/+}$ gallbladders in either the $Sox17^{+/-}$ or wild-type background (Fig. 5E).

In contrast to the lack of appreciable defects in the *Shh* mutant gallbladder epithelium, the formation of smooth muscle layers was considerably affected by the reduced dosage of *Sox17* and *Shh* (Fig. 5F,G). Anti-α smooth muscle actin (SMA) staining of wild-type embryos revealed that SMA-positive cells were detectable within the distal mesenchymal region of the gallbladder at ∼11.5 dpc, when they expand in a distal-to-proximal manner, leading to the formation of smooth muscle layers surrounding the gallbladder region, but not the cystic duct region, by 15.5 dpc (Fig. S11). In the $Sox17^{+/-}$, $Shh^{+/-}$ and $Shh^{-/-}$ embryos, anti-SMA staining showed reduced signal intensities in the gallbladder mesenchyme at 14.5 dpc (Fig. 5F), in which SMA-positive cells appear to be located randomly and discontinuously in the mesenchymal region around the epithelium (Fig. 5F, insets). At later stages, the $Shh^{+/-}$ gallbladders showed proper formation of the SMA-positive smooth muscle layer, similar to that of the wild-type

Development (2017) 144, 1906-1917 doi:10.1242/dev.147512

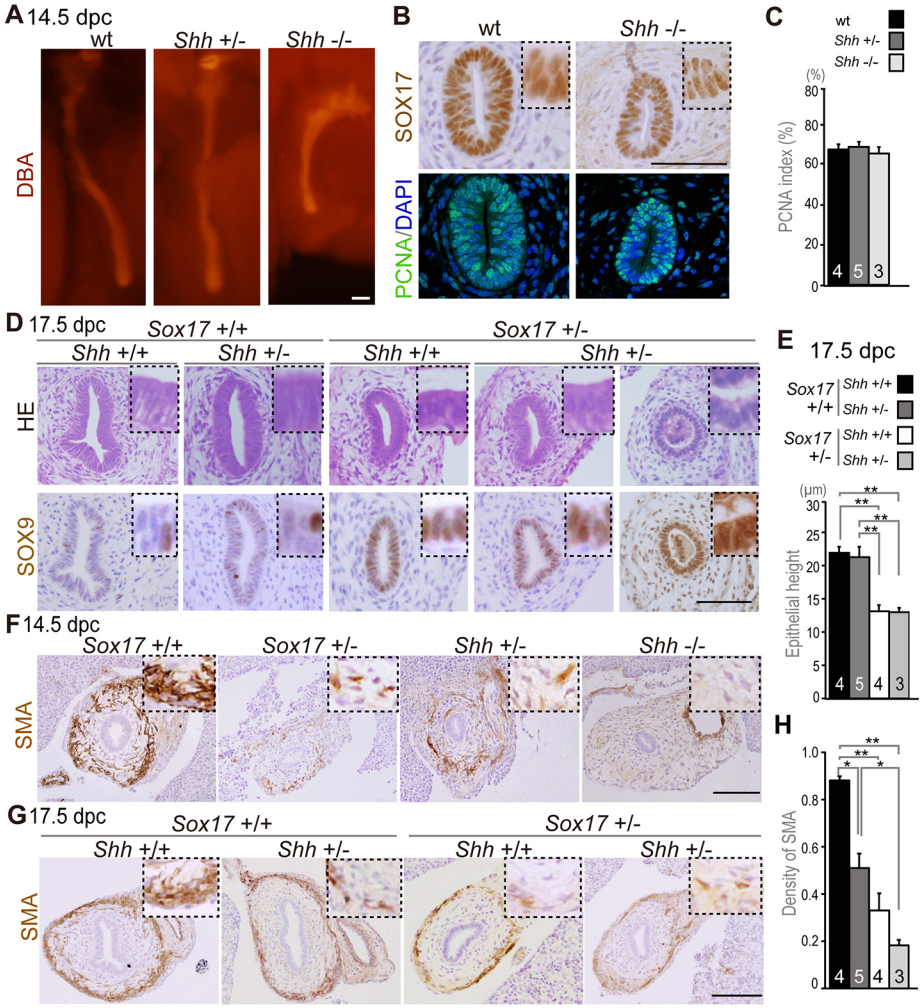

Fig. 5. *Sox17* and *Shh* coordinately regulate the proper formation of smooth muscles in the gallbladder. (A) Whole-mount DBA staining of wild-type, $Shh^{+/-}$ and $Shh^{-/-}$ liver with gallbladder and cystic duct. (B) Anti-SOX17 and anti-PCNA staining of serial transverse sections of wild-type and $Shh^{-/-}$ gallbladder at 14.5 dpc. (C) Quantitative analysis of the PCNA index (percentage PCNA-positive cells among total cells) in the gallbladder epithelium shows no differences among wild-type, $Shh^{+/-}$ and $Shh^{-/-}$ gallbladders at 14.5 dpc. (D) HE and anti-SOX9 staining in transverse sections of fetal gallbladders of wild-type, $Shh^{+/-}$, $Sox17^{+/-}$ and $Sox17^{+/-}$;$Shh^{+/-}$ embryos at 17.5 dpc. (E) Quantitative data from wild-type and $Sox17^{+/-}$ embryos at 17.5 dpc show no appreciable alteration in epithelial height of the gallbladder upon loss of one *Shh* allele. (F,G) Anti-SMA staining on transverse sections of the gallbladder in $Sox17^{+/-}$, $Shh^{+/-}$, $Shh^{-/-}$ and $Sox17^{+/-}$;$Shh^{+/-}$ embryos at 14.5 dpc (F) and 17.5 dpc (G). SMA-positive cells were patchy in the gallbladder mesenchyme and severely reduced in the $Shh^{-/-}$ gallbladder at 14.5 dpc. At 17.5 dpc, proper formation of the SMA-positive muscle layer was evident in $Shh^{+/-}$ embryos, whereas SMA-positive signals remained patchy in $Sox17^{+/-}$, $Shh^{+/-}$ and $Sox17^{+/-}$;$Shh^{+/-}$ gallbladders. (H) Quantitative data of SMA-positive signals show a gradual reduction in the $Shh^{+/-}$, $Sox17^{+/-}$ and $Sox17^{+/-}$;$Shh^{+/-}$ gallbladders. Insets are higher magnification images of SMA-positive cells in the gallbladder epithelia (B,D) and its surrounding mesenchyme (F,G). *P<0.05, **P<0.01, ANOVA followed by Tukey's test. Sample size is indicated within each bar. Scale bars: 100 µm.

gallbladder, in which SMA-positive cells completely surround the gallbladder epithelia (Fig. 5F, left two images). Both $Sox17^{+/-}$ and $Sox17^{+/-}$;$Shh^{+/-}$ embryos showed severely affected smooth muscle layers, in which SMA-positive cells appeared reduced and patchy in the surrounding mesenchyme (Fig. 5G, right two images). Morphometric analyses using anti-SMA staining revealed that the signal density was significantly reduced in the gallbladder mesenchyme of $Shh^{+/-}$, $Sox17^{+/-}$ or $Sox17^{+/-}$;$Shh^{+/-}$ embryos at 14.5 dpc, compared with that of wild-type embryos (Fig. 5H). Moreover, anti-SMA signals were more severely affected in $Sox17^{+/-}$;$Shh^{+/-}$ gallbladders than in $Shh^{+/-}$ gallbladders, albeit with no significant difference. These data suggest that the formation of smooth muscle layers in $Shh^{+/-}$ or $Sox17^{+/-}$ gallbladders is both delayed and defective, and this phenotype appears to be more severe in $Sox17^{+/-}$;$Shh^{+/-}$ gallbladders.

Fully active *Sox17* is required for proper formation of contractile smooth muscle layers of the gallbladder by the perinatal stage

To examine the contractile ability of the smooth muscle layers in the fetal gallbladder, we analyzed the network of smooth muscle cells in wild-type and $Sox17^{+/-}$ embryos at 17.5 dpc by whole-mount anti-SMA staining (Fig. 6). In the wild-type gallbladder, most of the smooth muscle fibers run in a circular direction (Fig. 6A), whereas in $Sox17^{+/-}$ gallbladders the smooth muscle cells appear to be distributed randomly and irregularly (Fig. 6B), with a swirling pattern distinct from that seen in the wild-type circular smooth muscle layer. This is consistent with the fragmented pattern of the smooth muscle layer observed in transverse sections (Fig. 5G).

Next we examined KCl-induced contraction (the relative changes in the maximum luminal diameter) of the fetal gallbladder in wild-type and $Sox17^{+/-}$ embryos with or without gross anatomical hepatic lesions (severe or mild phenotype group) at 17.5 dpc (Fig. 6C,D). In wild-type gallbladders, the KCl-induced contraction level was 87.4±1.9% (n=33; Fig. 6D). However, in the $Sox17^{+/-}$ gallbladder, KCl treatment caused no appreciable contraction: 94.2±2.9% (n=11) and 99.4±4.4% (n=12) in the mild and severe phenotype groups, respectively (Fig. 6D). In particular, the contraction level of the severe phenotype group was significantly reduced in the $Sox17^{+/-}$ gallbladders compared with wild type.

To examine non-induced muscle contraction in the fetal gallbladder at the perinatal stage *in vivo*, we isolated the liver and gallbladder from wild-type and $Sox17^{+/-}$ embryos at 17.5 dpc and measured the rate of autonomous gallbladder contraction under a dissection microscope for 10 min at room temperature. In wild-type gallbladders, the average rate of circular contractile movement was 0.48±0.28 times/min (n=5; Movie 1). This is in contrast to the rare and longitudinal muscle contraction in $Sox17^{+/-}$ gallbladders at 0.09±0.06 times/min (n=5; Movie 2). These data show that the defective formation of the circular smooth muscle layer affects muscle contractility in the $Sox17^{+/-}$ gallbladder. This might contribute to the onset of cholestasis and biliary atresia in the $Sox17^{+/-}$ mouse model.

Development (2017) 144, 1906-1917 doi:10.1242/dev.147512

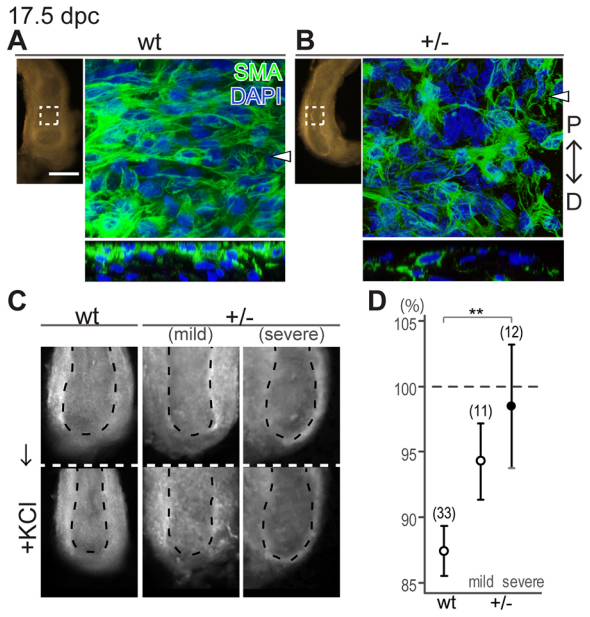

Fig. 6. Defective contraction of smooth muscles in *Sox17*$^{+/-}$ gallbladder. (A,B) Whole-mount anti-SMA staining of wild-type and *Sox17*$^{+/-}$ gallbladders at 17.5 dpc. (Top) Confocal *z*-projection from the area of the gallbladder indicated by the dashed box (left). (Bottom) Orthogonal projection in the *xz* plane made at the level of the arrowhead (above). The orientation of the discontinuous SMA-positive cells was randomized in the *Sox17*$^{+/-}$ gallbladder, in contrast to the dense SMA-positive fibers arranged mainly in a circular direction in the wild-type gallbladder. D, distal; P, proximal. (C,D) Dissection microscope images of the fetal gallbladder before (top) and after (bottom) KCl treatment (C) and KCl-induced contraction levels (relative changes in luminal diameter; D) of wild-type and the *Sox17*$^{+/-}$ gallbladder with (severe) or without (mild) gross anatomical hepatic lesions at 17.5 dpc. KCl treatment reduced luminal diameter considerably in the wild-type but not in the *Sox17*$^{+/-}$ gallbladder, with the severe phenotype group being particularly unaffected. Number of samples (gallbladders) are indicated. $^{**}P<0.01$, ANOVA followed by Tukey's test. Scale bar: 100 µm.

Ectopic SHH signaling rescues the defective formation of smooth muscle layers in the *Sox17*$^{+/-}$ gallbladder *in vitro*

Using an *in vitro* culture system in which each gallbladder is held within a single cylindrical groove of an agarose gel (Fig. 7A,B), we carried out a rescue experiment using recombinant SHH-soaked beads, which can weakly to moderately induce upregulation and downregulation of endogenous *Gli2* and *Shh* expression, respectively, in the 13.5 dpc gallbladder explants (Fig. S12). Wild-type gallbladder explants elongated in a distal-to-proximal manner to form a tubular structure along the cylindrical space within the agarose gel. Furthermore, these gallbladders displayed a well-developed pseudostratified columnar epithelium with epithelial folds (n=14/17; Fig. 7A,C, left), in addition to well-developed SMA-positive smooth muscle layers surrounding a SOX9-negative gallbladder epithelium (n=11/14; Fig. 7D,F, left). By contrast, the control (PBS) explants of *Sox17*$^{+/-}$ gallbladders displayed a single-layered cuboidal epithelium without any epithelial fold formation (n=12/12; Fig. 7C). The SMA-positive smooth muscle layer developed poorly around the SOX9-positive gallbladder epithelium (n=10/11; Fig. 7D), recapitulating the defective phenotypes of the *Sox17*$^{+/-}$ gallbladder *in vivo*. Interestingly, the addition of SHH-soaked beads rescued several of the *Sox17*$^{+/-}$ gallbladder phenotypes, resulting in a well developed smooth muscle layer organized around a pseudostratified epithelium (n=10/13; Fig. 7C,D, right two images). Morphometric analysis confirmed that the epithelial height and area of the luminal cavity in the *Sox17*$^{+/-}$ gallbladder were comparable to those of wild-type explants following SHH treatment (n=11; Fig. 7G). These findings suggest that reduced SHH signaling results in defective smooth muscle formation and epithelial fold formation in the *Sox17*$^{+/-}$ gallbladder.

In addition, ectopic SHH signaling had no appreciable effect on the percentage of PCNA-positive or Ki67-positive cells in the *Sox17*$^{+/-}$ gallbladder epithelium (Fig. 7E,H; Fig. S13), or on the number of ectopic SOX9-positive epithelial cells in the *Sox17*$^{+/-}$ gallbladder (epithelial area in Fig 7G, Fig. 7F,I). The *Sox17*$^{+/-}$ gallbladder explants showed shredding of some epithelial cells even *in vitro* (Fig. S14A; see also Fig. 7C, right, inset). However, the remaining *Sox17*$^{+/-}$ epithelial layer exhibits proper subcellular localization of both E-cadherin and ZO-1 (TJP1) even in the region near the damaged site (Fig. S14A). Moreover, the expression levels of *Cxcl10* and *Olfm4*, although not *Serpine1*, showed a tendency to increase in the *Sox17*$^{+/-}$ explants as compared with the wild-type explants (Fig. S14B), but such increased expression, at least of *Olfm4*, could not be rescued by SHH-soaked beads (Fig. S14B). These data suggest that most defective phenotypes in the *Sox17*$^{+/-}$ gallbladder epithelium are SHH independent. The present results are summarized in Fig. S15.

DISCUSSION

First, we demonstrated the presence of ectopic SOX9-positive cystic duct-like epithelia in the *Sox17*$^{+/-}$ gallbladder, together with the cooperatively increased expression of *Sox4*, which functions redundantly with *Sox9* in intrahepatic ducts (Poncy et al., 2015). *Sox9* is highly expressed in the cystic duct epithelium, in addition to the intrahepatic, pancreatic and common bile ducts (Furuyama et al., 2011). One possible explanation for the ectopic *Sox9*/*Sox4*-positive cystic duct epithelia in the proximal gallbladder region is an expansion of the cystic duct region toward the gallbladder domain as a consequence of the reduced proliferation and luminal deciduation of the *Sox17*$^{+/-}$ gallbladder epithelial cells (Uemura et al., 2013). However, the reduced epithelial proliferation is also observed in the cystic duct domain of the *Sox17*$^{+/-}$ gallbladder primordium, in addition to there being lower proliferative activity in the proximal cystic duct region than in the SOX17-positive distal region (Uemura et al., 2013). Although SOX17 and SOX9/SOX4 have similar sequence specificity in their DNA-binding HMG box domains (Kanai et al., 1996; Mertin et al., 1999), they have distinct characteristics for β-catenin binding and dimerization (Wilson and Koopman, 2002; Sinner et al., 2007; Kamachi and Kondoh, 2013). Hence, the cystic duct-like phenotype in the proximal *Sox17*$^{+/-}$ gallbladder might be caused partially by the appearance of ectopic SOX9/SOX4-positive cells in the bile duct epithelia, instead of by the loss of SOX17-positive cells. Further studies are required to more precisely define the hierarchy downstream of SOX17 or SOX9/SOX4 in the specification of the gallbladder and cystic duct epithelia of wild-type and *Sox17*$^{+/-}$ embryos.

By the perinatal stage, cystic duct-like *Sox17*$^{+/-}$ gallbladders showed increased expression of the inflammatory/cholestasis-associated markers *Abcb4* and *Olfm4*, in addition to *Cxcl10*, a key chemokine gene characteristic of the early immune response (Fig. 2C,D). The expression levels of several fetal myeloid cell markers also showed a tendency to increase in the *Sox17*$^{+/-}$ gallbladders, together with the enrichment of Gr1-positive or F4/80-positive myeloid-like cells in the gallbladder mesenchymal region (Fig. S6), suggesting fetal cholecystitis in *Sox17*$^{+/-}$ embryos. *Abcb4* encodes a lipid translocator for phosphatidylcholine, which

Development (2017) 144, 1906-1917 doi:10.1242/dev.147512

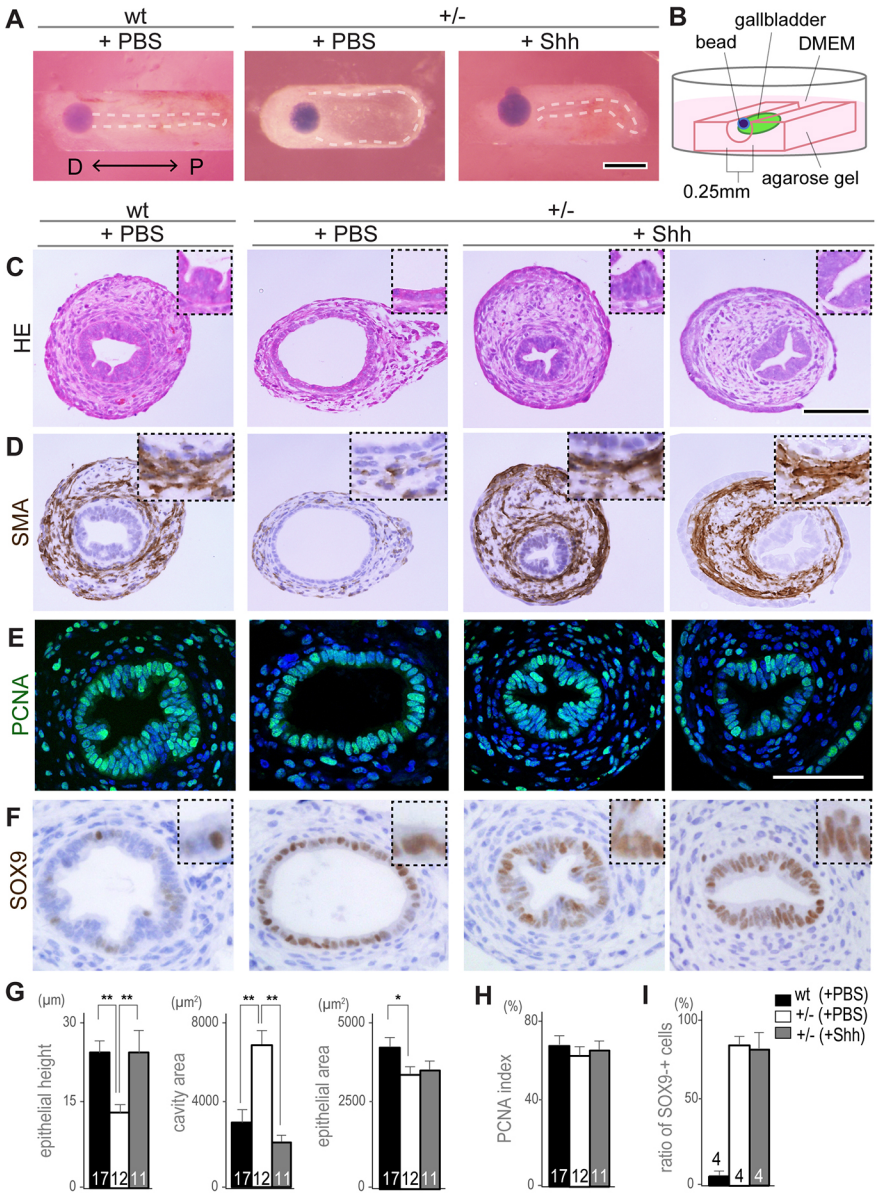

Fig. 7. Defective smooth muscle development of *Sox17*$^{+/-}$ gallbladders is rescued by exogenous SHH. (A,B) Three day organ culture of wild-type or *Sox17*$^{+/-}$ gallbladder primordium initiated at 13.5 dpc (A). The gallbladder and bead are held inside a single cylindrical groove of agarose gel as schematically represented in B. D, distal; P, proximal. (C-F) HE, anti-SMA, anti-PCNA or anti-SOX9 staining on transverse sections of wild-type or *Sox17*$^{+/-}$ gallbladder explants with PBS-soaked or SHH-soaked beads. Insets are higher magnification images of the epithelium or the signals. (G-I) Quantitative morphometric analysis of wild-type and *Sox17*$^{+/-}$ gallbladder explants cultured with PBS-soaked or SHH-soaked beads. Exogenous SHH signaling rescued the defects in epithelial height and cavity area, but did not exert any significant influence on epithelial area (G), PCNA index (H) or relative SOX9-positive cell numbers (I) within the gallbladder epithelium. **P*<0.05, ***P*<0.01, ANOVA followed by Tukey's test. Sample number is indicated with each bar. Scale bars: 100 μm.

transfers bile into bile salt micelles for the protection of the apical surface of the bile duct epithelia (Fickert et al., 2004; Esten Nakken et al., 2007; Baghdasaryan et al., 2011; Oude Elferink and Paulusma, 2007). *Abcb4* null mice display severe sclerosing or chronic cholangitis (Fickert et al., 2004; Esten Nakken et al., 2007; Baghdasaryan et al., 2011). Since a significant elevation of *ABCB4* was also reported in human patients with extrahepatic cholestasis (Schaap et al., 2009), *Abcb4* upregulation in *Sox17*$^{+/-}$ gallbladders *in vivo* might be caused partially by its adaptive response to minimize cellular damage by decreasing bile salt toxicity. *Olfm4* encodes a secreted protein with one olfactomedin-like domain (also known as an intestinal stem cell marker; Gersemann et al., 2012) and is upregulated in inflammatory bowel diseases such as ulcerative colitis and Crohn's disease (Liu et al., 2010; Gersemann et al., 2012). It is also possible that the *in vivo* upregulation of these bile duct disease markers is an effort to compensate for the defective barrier of the bile duct epithelia in the *Sox17*$^{+/-}$ gallbladder.

Genetic analysis demonstrated that embryonic hepatitis could be induced by a conditional *Sox17* deletion in the primordial gallbladder, but not in the liver hepatoblasts (Fig. 3; Fig. S7). The expression analysis of inflammatory markers also showed a positive correlation between cholecystitis and the severity of embryonic hepatitis in *Sox17*$^{+/-}$ embryos (Fig. 2D,E). These data suggest that the cholecystitis causes the biliary atresia and subsequent hepatic inflammation in *Sox17*$^{+/-}$ embryos. It is also possible that, at the late organogenesis stages of the extrahepatic bile ducts, the inflammatory responses of the bile duct epithelia and its surrounding mesenchymal tissues cause severe defects in both bile duct morphogenesis and epithelial barrier function, leading to increased bile leakage and inflammatory responses in the fetal gallbladder by 17.5 dpc.

The present genetic and *in vitro* rescue experiments revealed that SHH signaling may be crucial for the proper formation of smooth muscles downstream of *Sox17* in the normal development of the gallbladder during the late organogenesis stages. HH signaling in the endodermal epithelium plays a major role in the mesenchymal development of the digestive tract. Loss of HH signaling has also been shown to decrease cell proliferation in the underlying mesenchyme, resulting in thinner walls of the stomach and

Development (2017) 144, 1906-1917 doi:10.1242/dev.147512

intestine (Mao et al., 2010; reviewed by van den Brink, 2007). Moreover, SHH signaling enhances smooth muscle formation in the intestine, lung, and urinary bladder via other molecules, including Ptch and Gli family members (Apelqvist et al., 1997; Li et al., 2004; Caubit et al., 2008; DeSouza et al., 2013), suggesting that smooth muscle cells might be a target of SHH signaling. These previous reports help to explain the delayed and aberrant formation of smooth muscle layers in the developing *Sox17*$^{+/-}$ gallbladder, and they are also consistent with several previous reports showing deficient smooth muscle layers in the fetal gallbladder caused by *Foxf1* haploinsufficiency, a downstream mediator of HH signaling, in mouse organogenesis stage embryos (Kalinichenko et al., 2002; Madison et al., 2009).

It was recently suggested that the deformation, inflammation and repair processes of the bile ducts are closely associated with SHH signaling. For example, Jung et al. (2015) reported that SHH pathway activation was observed, especially in the cholangiocytes of the peribiliary glands, in human patients with biliary atresia. In pathological studies, some have reported that *Hh* expression is considerably increased in fibrotic damaged biliary diseases in response to injury (Omenetti et al., 2008; Omenetti and Diehl, 2011; Cui et al., 2013; Hu et al., 2015). It has also been speculated that the SHH signaling pathway regulates the epithelial-mesenchymal transition of cholangiocytes (Omenetti et al., 2008; Jung et al., 2015). The effects of excess SHH signaling encompass defective hepatobiliary ducts in a zebrafish model (Cui et al., 2013; Tang et al., 2016), suggesting that excess SHH signaling can have detrimental effects on the proper development and maintenance of the biliary duct. The current phenotype of reduced SHH signaling in the defective gallbladder might be explained by the distinct roles of SHH signaling during developmental and early pathogenic stages (i.e. smooth muscle layer formation and tubulogenesis) versus late pathogenic and inflammatory processes (i.e. transdifferentiation of damaged mesenchymal cells into smooth muscle cells for tissue repair). It is also possible that SHH signaling must be maintained at an appropriate level, since both excess and reduced SHH signaling may possibly lead to defective formation and maintenance of the biliary duct system.

Finally, the present study has shown defective gallbladder contraction in *Sox17*$^{+/-}$ perinatal embryos (Fig. 6; Movies 1 and 2). In particular, *Sox17*$^{+/-}$ gallbladders with hepatic lesions have severe defects in contraction, suggesting a potential contribution of the defective muscle layers to the onset of cholestasis in the *Sox17*$^{+/-}$ embryos soon after the first biliary excretion into the fetal duodenum. Since well-developed smooth muscle layers are restricted to the gallbladder wall, in contrast to poor formation of the smooth muscle layers around the cystic and common bile ducts (Higashiyama et al., 2016 and references therein), the defective gallbladder contraction directly affects the flow of bile from the fetal gallbladder into the duodenum in the *Sox17*$^{+/-}$ embryos. This symptom is also consistent with the ultrasonographic diagnostic features for human biliary atresia, such as the 'non-contractile' gallbladder with its reduced length, irregular wall and indistinct mucosal lining (Kanegawa et al., 2003). Further studies are required to establish the contribution of fetal gallbladder contraction in the onset of biliary atresia-like syndrome in individual *Sox17*$^{+/-}$ embryos.

MATERIALS AND METHODS

Animal care and use

Animal experiments were performed in strict accordance with the Guidelines for Animal Use and Experimentation established by the University of Tokyo (approval ID: P13-763, P14-877), the Tokyo Medical and Dental University (approval ID: 0140007A, 0150259C2, 0160024C2, 0170248C2) and the University of Utah (approval ID: 14-01003). The *Sox17*$^{+/-}$ embryos at F9-10 generation were obtained from wild-type females [C57BL6 (B6) strain; Clea, Japan] mated with the *Sox17*$^{+/-}$ male mice (Kanai-Azuma et al., 2002), which were intercrossed and maintained at F8-9 backcross generation to the B6 strain. In this mating system, the *Sox17*$^{+/-}$ embryos (F9-10) show ∼70% neonatal lethality, while the remaining survivors can be grown until adulthood without any signs of hepatitis, albeit with a small gallbladder. *Sox17*$^{+/-(GFP)}$, *Sox17* $^{flox/flox}$ (B6×129sv background; 13.5-17.5 dpc) (Kim et al., 2007), *Alb*-cre (Postic et al., 1999), *Pdx1*-cre (Hingorani et al., 2003) and *Shh*$^{+/-(GFP)}$ (Harfe et al., 2004) mice were also used in this study.

Histology, immunohistochemistry and whole-mount *in situ* hybridization

Tissues were fixed in 4% paraformaldehyde in PBS for 12 h at 4°C. For sections, the fixed samples were embedded in paraffin and serially sectioned (4 µm thick). For comparative analyses of transverse sections of the gallbladder, sections at the level of maximum diameter (at least four sections in each individual sample) were used. Immunohistochemistry was conducted by a standard protocol (see the supplementary Materials and Methods) and *in situ* hybridization was performed as described by Hiramatsu et al. (2009). Details of reagents and methods are provided in the supplementary Materials and Methods.

Measurement of length, area and signal density

For length and area measurements, ImageJ 1.48V software (National Institutes of Health, USA) was used. For measurement of signal density of anti-SMA-stained sections, we conducted grid analyses of the HRP-positive reactions. A grid (each box=10×10 µm) was overlaid on the image of the stained section and the signal density (d) calculated by d=b/(a+b), where (a) the signal passed through more than two sides of the box and (b) the signal was fragmented or passed through one side of the box.

RNA extraction, microarray and qPCR analyses

The *Sox17*$^{+/-}$ and wild-type gallbladders at 15.5 dpc were used for microarray expression analysis according to the method developed by Huang et al. (2009a,b). GSEA was carried out according to Subramanian et al. (2005). qPCR analysis was used to determine marker gene expression levels relative to *Gapdh*. Details of these methods are provided in the supplementary Materials and Methods.

Monitoring the contractile movement of fetal gallbladder

Whole livers, including the gallbladder and biliary tract (17.5 dpc), were maintained in 10% fetal calf serum-DMEM (Sigma) at 37°C, and prepared for time-lapse imaging using a dissection microscope (Olympus SZX16) equipped with a video recording system (Olympus DP71 camera; imaged every 2 s for a total of 10 min). Each gallbladder was separated from the liver and imaged before and after 45 mM KCl treatment for 10 min. Maximum luminal diameter of the gallbladder before and after KCl was measured using ImageJ 1.48V, and the relative change in maximum luminal diameter estimated as an indication of gallbladder contraction.

Organ culture

The gallbladder was isolated from the fetal liver using a dissection microscope at 13.5 dpc. To apply the pressure that would normally be exerted by the liver and to promote directional growth, the gallbladders were placed in a groove of a 1.5% agarose gel plate prepared using a stainless steel needle of 0.26 mm diameter, which is similar to the liver gap around the gallbladder at 16.5 dpc (see Fig. 7B). Beads soaked in mouse recombinant SHH (1 mg/ml; SRP6004, Sigma) or PBS were placed on the distal tip of the gallbladder and cultured in 10% fetal calf serum-DMEM at 37°C for 72 h.

Statistical analyses

All quantitative data are represented as mean±s.e.m. Student's *t*-test, Mann–Whitney U-test and ANOVA tests were used to determine overall differences between two groups or among more than two groups. Where differences existed, Tukey's test was also used to compare each value with

Development (2017) 144, 1906-1917 doi:10.1242/dev.147512

every other value. The correlation between genes/groups in both gallbladder and liver samples was estimated using Spearman's rank correlation test. $P<0.05$ was considered statistically significant.

Acknowledgements
We thank Drs A. Asai, S. Elliott, K. Nakamura and A. Tanoue for critical reading of the manuscript; Prof. Dr S. J. Morrison for providing *Sox17*$^{+/-(GFP)}$ mice; and Dr M. Kawasumi, Y. Kuroda, Ms Y. Uchiyama and I. Yagihashi for helpful support.

Competing interests
The authors declare no competing or financial interests.

Author contributions
Conceptualization: H.H., N.T., Y.K.; Methodology: H.H., A.O., H.S., M.U., K.I., Y.S.; Software: A.O., H.S.; Validation: H.H., A.O., H.S., M.U.; Formal analysis: H.H., A.O., H.S., M.U., H.I.; Investigation: H.H., A.O., H.S., M.U., N.T.; Resources: H.H., A.O., M.U., K.F., H.I., Y.H., M.K., Y.S., M.K.-A.; Data curation: H.H., A.O., H.S., M.U., K.F., Y.H., Y.S.; Writing - original draft: H.H.; Writing - review & editing: H.H., M.K., M.K.-A., Y.K.; Visualization: H.H., K.I.; Supervision: M.K., Y.K.; Project administration: Y.K.; Funding acquisition: Y.K.

Funding
This work was supported mainly by grants from the Ministry of Education, Culture, Sports, Science, and Technology of Japan to Y.K. (S-24228005) and M.K.-A. (C-24500485). This work was also supported by a grant from the National Institute of Child Health and Human Development to Y.S. (R01 HD066121). Deposited in PMC for release after 12 months.

Data availability
Microarray data are available at NCBI Gene Expression Omnibus under accession number GSE74576.

Supplementary information
Supplementary information available online at
http://dev.biologists.org/lookup/doi/10.1242/dev.147512.supplemental

References
Apelqvist, Å., Ahlgren, U. and Edlund, H. (1997). Sonic hedgehog directs specialised mesoderm differentiation in the intestine and pancreas. *Curr. Biol.* **7**, 801-804.

Asai, A., Miethke, A. and Bezerra, J. A. (2015). Pathogenesis of biliary atresia: defining biology to understand clinical phenotypes. *Nat. Rev. Gastroenterol. Hepatol.* **12**, 342-352.

Baghdasaryan, A., Claudel, T., Gumhold, J., Silbert, D., Adorini, L., Roda, A., Vecchiotti, S., Gonzalez, F. J., Schoonjans, K. and Strazzabosco, M. (2011). Dual farnesoid X receptor/TGR5 agonist INT-767 reduces liver injury in the *Mdr2*$^{-/-}$ (*Abcb4*$^{-/-}$) mouse cholangiopathy model by promoting biliary HCO_3^- output. *Hepatology* **54**, 1303-1312.

Bessho, K., Mourya, R., Shivakumar, P., Walters, S., Magee, J. C., Rao, M., Jegga, A. G. and Bezerra, J. A. (2014). Gene expression signature for biliary atresia and a role for interleukin-8 in pathogenesis of experimental disease. *Hepatology* **60**, 211-223.

Caubit, X., Lye, C. M., Martin, E., Core, N., Long, D. A., Vola, C., Jenkins, D., Garratt, A. N., Skaer, H., Woolf, A. S. et al. (2008). Teashirt 3 is necessary for ureteral smooth muscle differentiation downstream of SHH and BMP4. *Development* **135**, 3301-3310.

Cui, S., Leyva-Vega, M., Tsai, E. A., EauClaire, S. F., Glessner, J. T., Hakonarson, H., Devoto, M., Haber, B. A., Spinner, N. B. and Matthews, R. P. (2013). Evidence from human and zebrafish that *GPC1* is a biliary atresia susceptibility gene. *Gastroenterology* **144**, 1107-1115.

Davenport, M. (2016). Biliary atresia: from Australia to the zebrafish. *J. Pediatr. Surg.* **51**, 200-205.

Desmet, V. J. (1992). Congenital diseases of intrahepatic bile ducts: variations on the theme "ductal plate malformation". *Hepatology* **16**, 1069-1083.

DeSouza, K. R., Saha, M., Carpenter, A. R., Scott, M. and McHugh, K. M. (2013). Analysis of the Sonic Hedgehog signaling pathway in normal and abnormal bladder development. *PLoS ONE* **8**, e53675.

Echelard, Y., Epstein, D. J., St-Jacques, B., Shen, L., Mohler, J., McMahon, J. A. and McMahon, A. P. (1993). Sonic hedgehog, a member of a family of putative signaling molecules, is implicated in the regulation of CNS polarity. *Cell* **75**, 1417-1430.

Emig, D., Salomonis, N., Baumbach, J., Lengauer, T., Conklin, B. R. and Albrecht, M. (2010). AltAnalyze and DomainGraph: analyzing and visualizing exon expression data. *Nucleic Acids Res.* **38** Suppl., W755-W762.

Esten Nakken, K., Nygård, S., Haaland, T., Erik Berge, K., Arnkvaern, K., Ødegaard, A., Jørgen Labori, K. and Ræder, M. G. (2007). Multiple inflammatory-, tissue remodelling-and fibrosis genes are differentially transcribed in the livers of *Abcb4* (-/-) mice harbouring chronic cholangitis. *Scandinav. J. Gastroenterol.* **42**, 1245-1255.

Fickert, P., Fuchsbichler, A., Wagner, M., Zollner, G., Kaser, A., Tilg, H., Krause, R., Lammert, F., Langner, C., Zatloukal, K. et al. (2004). Regurgitation of bile acids from leaky bile ducts causes sclerosing cholangitis in *Mdr2* (*Abcb4*) knockout mice. *Gastroenterology* **127**, 261-274.

Furuyama, K., Kawaguchi, Y., Akiyama, H., Horiguchi, M., Kodama, S., Kuhara, T., Hosokawa, S., Elbahrawy, A., Soeda, T., Koizumi, M. et al. (2011). Continuous cell supply from a *Sox9*-expressing progenitor zone in adult liver, exocrine pancreas and intestine. *Nat. Genet.* **43**, 34-41.

Gersemann, M., Becker, S., Nuding, S., Antoni, L., Ott, G., Fritz, P., Oue, N., Yasui, W., Wehkamp, J. and Stange, E. F. (2012). Olfactomedin-4 is a glycoprotein secreted into mucus in active IBD. *J. Crohns Colitis* **6**, 425-434.

Gordo-Gilart, R., Andueza, S., Hierro, L., Martinez-Fernández, P., D'Agostino, D., Jara, P. and Alvarez, L. (2015). Functional analysis of ABCB4 mutations relates clinical outcomes of progressive familial intrahepatic cholestasis type 3 to the degree of MDR3 floppase activity. *Gut* **64**, 147-155.

Harfe, B. D., Scherz, P. J., Nissim, S., Tian, H., McMahon, A. P. and Tabin, C. J. (2004). Evidence for an expansion-based temporal Shh gradient in specifying vertebrate digit identities. *Cell* **118**, 517-528.

Hartley, J. L., O'Callaghan, C., Rossetti, S., Consugar, M., Ward, C. J., Kelly, D. A. and Harris, P. C. (2011). Investigation of primary cilia in the pathogenesis of biliary atresia. *J. Pediatr. Gastroenterol. Nutr.* **52**, 485-488.

Higashiyama, H., Sumitomo, H., Ozawa, A., Igarashi, H., Tsunekawa, N., Kurohmaru, M. and Kanai, Y. (2016). Anatomy of the murine hepatobiliary system: a whole-organ-level analysis using a transparency method. *Anat. Rec.* **299**, 161-172.

Hingorani, S. R., Petricoin, E. F., Maitra, A., Rajapakse, V., King, C., Jacobetz, M. A., Ross, S., Conrads, T. P., Veenstra, T. D., Hitt, B. A. et al. (2003). Preinvasive and invasive ductal pancreatic cancer and its early detection in the mouse. *Cancer Cell* **4**, 437-450.

Hiramatsu, R., Matoba, S., Kanai-Azuma, M., Tsunekawa, N., Katoh-Fukui, Y., Kurohmaru, M., Morohashi, K.-i, Wilhelm, D., Koopman, P. and Kanai, Y. (2009). A critical time window of Sry action in gonadal sex determination in mice. *Development* **136**, 129-138.

Hu, L., Lin, X., Lu, H., Chen, B. and Bai, Y. (2015). An overview of hedgehog signaling in fibrosis. *Mol. Pharmacol.* **87**, 174-182.

Huang, D. W., Sherman, B. T. and Lempicki, R. A. (2009a). Systematic and integrative analysis of large gene lists using DAVID bioinformatics resources. *Nat. Protoc.* **4**, 44-57.

Huang, D. W., Sherman, B. T. and Lempicki, R. A. (2009b). Bioinformatics enrichment tools: paths toward the comprehensive functional analysis of large gene lists. *Nucleic Acids Res.* **37**, 1-13.

Jung, H. Y., Jing, J., Lee, K. B. and Jang, J. J. (2015). Sonic hedgehog (SHH) and glioblastoma-2 (Gli-2) expressions are associated with poor jaundice-free survival in biliary atresia. *J. Pediatr. Surg.* **50**, 371-376.

Kalinichenko, V. V., Zhou, Y., Bhattacharyya, D., Kim, W., Shin, B., Bambal, K. and Costa, R. H. (2002). Haploinsufficiency of the mouse *Forkhead Box f1* gene causes defects in gall bladder development. *J. Biol. Chem.* **277**, 12369-12374.

Kamachi, Y. and Kondoh, H. (2013). Sox proteins: regulators of cell fate specification and differentiation. *Development* **140**, 4129-4144.

Kanai, Y., Kanai-Azuma, M., Noce, T., Saido, T. C., Shiroishi, T., Hayashi, Y. and Yazaki, K. (1996). Identification of two *Sox17* messenger RNA isoforms, with and without the high mobility group box region, and their differential expression in mouse spermatogenesis. *J. Cell Biol.* **133**, 667-681.

Kanai-Azuma, M., Kanai, Y., Gad, J. M., Tajima, Y., Taya, C., Kurohmaru, M., Sanai, Y., Yonekawa, H., Yazaki, K., Tam, P. P. et al. (2002). Depletion of definitive gut endoderm in Sox17-null mutant mice. *Development* **129**, 2367-2379.

Kanegawa, K., Akasaka, Y., Kitamura, E., Nishiyama, S., Muraji, T., Nishijima, E., Satoh, S. and Tsugawa, C. (2003). Sonographic diagnosis of biliary atresia in pediatric patients using the "triangular cord" sign versus gallbladder length and contraction. *Am. J. Roentgenology* **181**, 1387-1390.

Kelliher, M. A., Seldin, D. C. and Leder, P. (1996). Tal-1 induces T cell acute lymphoblastic leukemia accelerated by casein kinase IIalpha. *EMBO J.* **15**, 5160-5166.

Kidokoro, T., Matoba, S., Hiramatsu, R., Fujisawa, M., Kanai-Azuma, M., Taya, C., Kurohmaru, M., Kawakami, H., Hayashi, Y., Kanai, Y. et al. (2005). Influence on spatiotemporal patterns of a male-specific *Sox9* activation by ectopic *Sry* expression during early phases of testis differentiation in mice. *Dev. Biol.* **278**, 511-525.

Kim, I., Saunders, T. L. and Morrison, S. J. (2007). *Sox17* dependence distinguishes the transcriptional regulation of fetal from adult hematopoietic stem cells. *Cell* **130**, 470-483.

Kohsaka, T., Yuan, Z. R., Guo, S. X., Tagawa, M., Nakamura, A., Nakano, M., Kawasasaki, H., Inomata, Y., Tanaka, K. and Miyauchi, J. (2002). The significance of human jagged 1 mutations detected in severe cases of extrahepatic biliary atresia. *Hepatology* **36**, 904-912.

Leonhardt, J., Stanulla, M., von Wasielewski, R., Skokowa, J., Kübler, J., Ure, B. M. and Petersen, C. (2006). Gene expression profile of the infective murine model for biliary atresia. *Pediatr. Surg. Int.* **22**, 84-89.
Li, Y., Zhang, H., Choi, S. C., Litingtung, Y. and Chiang, C. (2004). Sonic hedgehog signaling regulates Gli3 processing, mesenchymal proliferation, and differentiation during mouse lung organogenesis. *Dev. Biol.* **270**, 214-231.
Liu, C. Z., Yang, J. T., Yoon, J. W., Villavicencio, E., Pfendler, K., Walterhouse, D. and Iannaccone, P. (1998). Characterization of the promoter region and genomic organization of *GLI*, a member of the *Sonic hedgehog-Patched* signaling pathway. *Gene* **209**, 1-11.
Liu, W., Yan, M., Liu, Y., Wang, R., Li, C., Deng, C., Singh, A., Coleman, W. G., Jr and Rodgers, G. P. (2010). Olfactomedin 4 down-regulates innate immunity against *Helicobacter pylori* infection. *Proc. Natl. Acad. Sci. USA* **107**, 11056-11061.
Lorent, K., Gong, W., Koo, K. A., Waisbourd-Zinman, O., Karjoo, S., Zhao, X., Sealy, I., Kettleborough, R. N., Stemple, D. L., Windsor, P. A., Whittaker, S. J., Porter, J. R., Wells, R. G., and Pack, M. et al. (2015). Identification of a plant isoflavonoid that causes biliary atresia. *Sci. Transl. Med.* **7**, 286ra67.
Mack, C. L. and Sokol, R. J. (2005). Unraveling the pathogenesis and etiology of biliary atresia. *Pediatr. Res.* **57**, 87R-94R.
Madison, B. B., McKenna, L. B., Dolson, D., Epstein, D. J. and Kaestner, K. H. (2009). FoxF1 and FoxL1 link hedgehog signaling and the control of epithelial proliferation in the developing stomach and intestine. *J. Biol. Chem.* **284**, 5936-5944.
Mao, J., Kim, B. M., Rajurkar, M., Shivdasani, R. A. and McMahon, A. P. (2010). Hedgehog signaling controls mesenchymal growth in the developing mammalian digestive tract. *Development* **137**, 1721-1729.
McConnell, B. B. and Yang, V. W. (2010). Mammalian Krüppel-like factors in health and diseases. *Physiol. Rev.* **90**, 1337-1381.
Mertin, S., McDowall, S. G. and Harley, V. R. (1999). The DNA-binding specificity of SOX9 and other SOX proteins. *Nucleic Acids Res.* **27**, 1359-1364.
Mieli-Vergani, G. and Vergani, D. (2009). Biliary atresia. *Semin. Immunopathol.* **31**, 371-381.
Motoyama, J., Heng, H., Crackower, M. A., Takabatake, T., Takeshima, K., Tsui, L.-C. and Hui, C.-c. (1998). Overlapping and non-overlapping Ptch2 expression with Shh during mouse embryogenesis. *Mech. Dev.* **78**, 81-84.
Nakagawa, M. and Setchell, K. D. (1990). Bile acid metabolism in early life: studies of amniotic fluid. *J. Lipid Res.* **31**, 1089-1098.
Nakamura, K. and Tanoue, A. (2013). Etiology of biliary atresia as a developmental anomaly: recent advances. *J. Hepatobiliary Pancreat. Sci.* **20**, 459-464.
Nakamura, M., Yasunami, M., Kondo, H., Horie, H., Aiba, Y., Komori, A., Migita, K., Yatsuhashi, H., Ito, M., Shimoda, S. et al. (2010). Analysis of *HLA-DRB1* polymorphisms in Japanese patients with primary biliary cirrhosis (PBC): the HLA-DRB1 polymorphism determines the relative risk of antinuclear antibodies for disease progression in PBC. *Hepatol. Res.* **40**, 494-504.
Okada, K., Kamiya, A., Ito, K., Yanagida, A., Ito, H., Kondou, H., Nishina, H. and Nakauchi, H. (2012). Prospective isolation and characterization of bipotent progenitor cells in early mouse liver development. *Stem Cells Dev.* **21**, 1124-1133.
Omenetti, A. and Diehl, A. M. (2011). Hedgehog signaling in cholangiocytes. *Curr. Opin. Gastroenterol.* **27**, 268-275.
Omenetti, A., Popov, Y., Jung, Y., Choi, S. S., Witek, R. P., Yang, L., Brown, K. D., Schuppan, D. and Diehl, A. M. (2008). The hedgehog pathway regulates remodelling responses to biliary obstruction in rats. *Gut* **57**, 1275-1282.
Oude Elferink, R. P. and Paulusma, C. C. (2007). Function and pathophysiological importance of ABCB4 (MDR3 P-glycoprotein). *Pflugers Arch.* **453**, 601-610.
Park, M. H., Jo, M., Kim, Y. R., Lee, C.-K. and Hong, J. T. (2016). Roles of peroxiredoxins in cancer, neurodegenerative diseases and inflammatory diseases. *Pharmacol. Therap.* **163**, 1-23.
Poncy, A., Antoniou, A., Cordi, S., Pierreux, C. E., Jacquemin, P. and Lemaigre, F. P. (2015). Transcription factors SOX4 and SOX9 cooperatively control development of bile ducts. *Dev. Biol.* **404**, 136-148.
Portincasa, P., Di Ciaula, A. and van Berge-Henegouwen, G. P. (2004). Smooth muscle function and dysfunction in gallbladder disease. *Curr. Gastroenterol. Rep.* **6**, 151-162.
Portincasa, P., Di Ciaula, A., Wang, H. H., Palasciano, G., van Erpecum, K. J., Moschetta, A. and Wang, D.-Q. (2008). Coordinate regulation of gallbladder motor function in the gut-liver axis. *Hepatology* **47**, 2112-2126.
Postic, C., Shiota, M., Niswender, K. D., Jetton, T. L., Chen, Y., Moates, J. M., Shelton, K. D., Lindner, J., Cherrington, A. D. and Magnuson, M. A. (1999). Dual roles for glucokinase in glucose homeostasis as determined by liver and pancreatic beta cell-specific gene knock-outs using Cre recombinase. *J. Biol. Chem.* **274**, 305-315.
Schaap, F. G., van der Gaag, N. A., Gouma, D. J. and Jansen, P. L. M. (2009). High expression of the bile salt-homeostatic hormone fibroblast growth factor 19 in the liver of patients with extrahepatic cholestasis. *Hepatology* **49**, 1228-1235.
Sinner, D., Kordich, J. J., Spence, J. R., Opoka, R., Rankin, S., Lin, S.-C. J., Jonatan, D., Zorn, A. M. and Wells, J. M. (2007). Sox17 and Sox4 differentially regulate β-catenin/T-cell factor activity and proliferation of colon carcinoma cells. *Mol. Cell. Biol.* **27**, 7802-7815.
Spence, J. R., Lange, A. W., Lin, S.-C. J., Kaestner, K. H., Lowy, A. M., Kim, I., Whitsett, J. A. and Wells, J. M. (2009). Sox17 regulates organ lineage segregation of ventral foregut progenitor cells. *Dev. Cell* **17**, 62-74.
Subramanian, A., Tamayo, P., Mootha, V. K., Mukherjee, S., Ebert, B. L., Gillette, M. A., Paulovich, A., Pomeroy, S. L., Golub, T. R., Lander, E. S. et al. (2005). Gene set enrichment analysis: a knowledge-based approach for interpreting genome-wide expression profiles. *Proc. Nat. Acad. Sci. USA* **102**, 15545-15550.
Tam, P. P., Kanai-Azuma, M. and Kanai, Y. (2003). Early endoderm development in vertebrates: lineage differentiation and morphogenetic function. *Curr. Opin. Genet. Dev.* **13**, 393-400.
Tan, C. E. L., Davenport, M., Driver, M. and Howard, E. R. (1994). Does the morphology of the extrahepatic biliary remnants in biliary atresia influence survival? A review of 205 cases. *J. Pediatr. Surg.* **29**, 1459-1464.
Tang, V., Cofer, Z. C., Cui, S., Sapp, V., Loomes, K. M. and Matthews, R. P. (2016). Loss of a candidate biliary atresia susceptibility gene, *add3a*, causes biliary developmental defects in zebrafish. *J. Pediatr. Gastroenterol. Nutr.* **63**, 524-530.
Uemura, M., Hara, K., Shitara, H., Ishii, R., Tsunekawa, N., Miura, Y., Kurohmaru, M., Taya, C., Yonekawa, H., Kanai-Azuma, M. et al. (2010). Expression and function of mouse *Sox17* gene in the specification of gallbladder/bile-duct progenitors during early foregut morphogenesis. *Biochem. Biophys. Res. Commun.* **391**, 357-363.
Uemura, M., Ozawa, A., Nagata, T., Kurasawa, K., Tsunekawa, N., Nobuhisa, I., Taga, T., Hara, K., Kudo, A., Kawakami, H. et al. (2013). *Sox17* haploinsufficiency results in perinatal biliary atresia and hepatitis in C57BL/6 background mice. *Development* **140**, 639-648.
van den Brink, G. R. (2007). Hedgehog signaling in development and homeostasis of the gastrointestinal tract. *Physiol. Rev.* **87**, 1343-1375.
Waisbourd-Zinman, O., Koh, H., Tsai, S., Lavrut, P.-M., Dang, C., Zhao, X., Pack, M., Cave, J., Hawes, M., Koo, K. A. et al. (2016). The toxin biliatresone causes mouse extrahepatic cholangiocyte damage and fibrosis through decreased glutathione and SOX17. *Hepatology* **64**, 880-893.
Wilson, M. and Koopman, P. (2002). Matching SOX: partner proteins and co-factors of the SOX family of transcriptional regulators. *Curr. Opin. Genet. Dev.* **12**, 441-446.

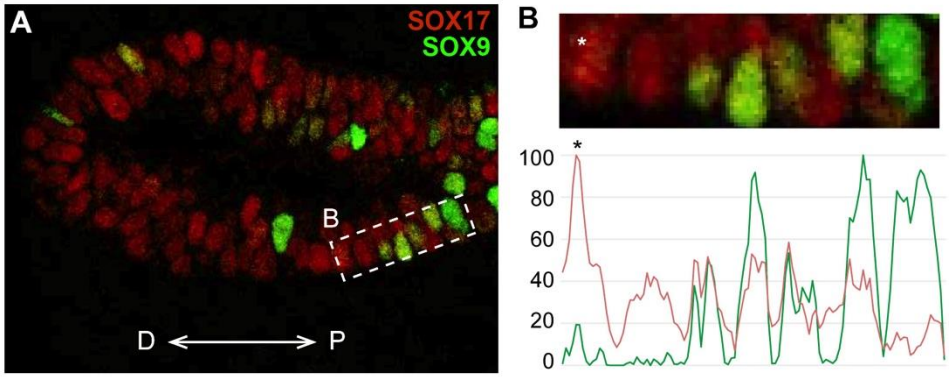

Fig. S1. The immunofluorescent images and signal intensities of SOX17 (red) and SOX9 (green) in the gallbladder epithelia in the 13.5-dpc wildtype embryo

(A) The SOX17-positive cells (red) are in the distal region of the primordial gallbladder, while the SOX9-positive cells (green) are in the proximal region near the cystic duct. **(B)** The immunofluorescent image and its intensities of the SOX17 (red) and SOX9 (green) signals in the transitional region. The SOX17 expression levels (set as 100% in the SOX17-positive cell at left-most side; asterisk) are reduced in the five SOX9-positive cells (upper plate) corresponding to the five peaks (lower plate) at right-hand side.

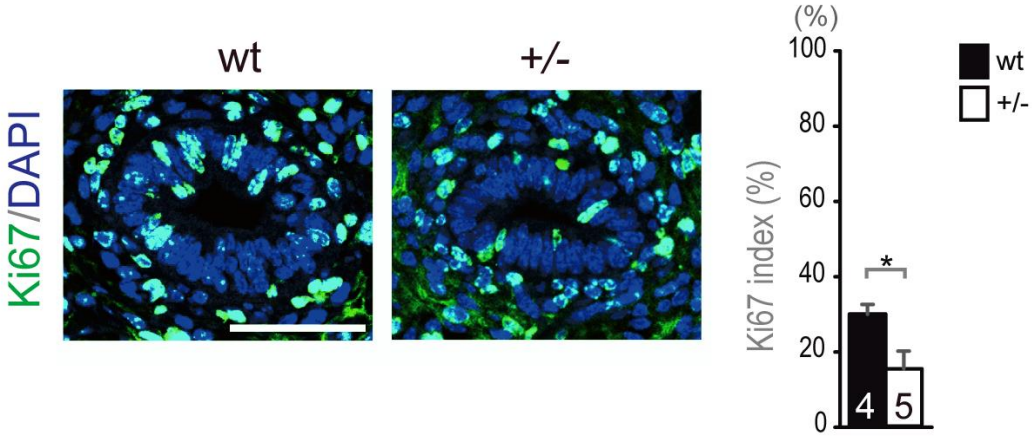

Fig. S2. Reduced Ki67-positive indices in cystic duct domain of *Sox17*$^{+/-}$ gallbladder primordia

The anti-Ki67 staining of the serial transverse sections of the presumptive cystic duct (Sox9-positive) domain in the *Sox17*$^{+/-}$ gallbladder at 15.5 dpc. The quantitative data of the Ki67-positive index show significant reduction in *Sox17*$^{+/-}$ epithelia than wild-type ones (*p<0.05). Scale bar: 100 μm.

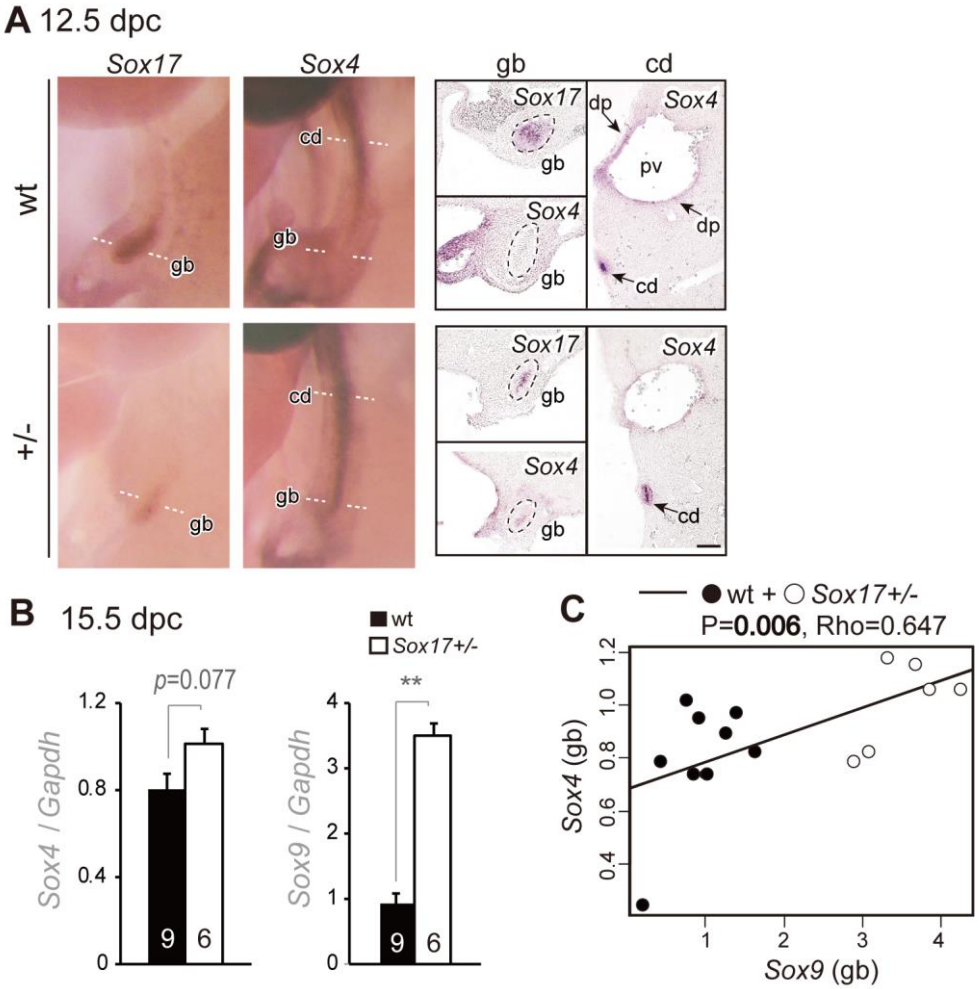

Fig. S3. The expression profiles of *Sox4* and *Sox9* in the fetal gallbladder and cystic duct of wild-type and *Sox17*$^{+/-}$ embryos

(A) The whole-mount *in situ* hybridization and their sectioning images at the levels of the gallbladder (gb) and cystic duct (cd) (indicated by the dotted lines in the left plates), showing the expression profiles of *Sox17* and *Sox4* in wild-type (wt) and *Sox17*$^{+/-}$ (+/-) embryos at 12.5 dpc. The *Sox4* expression domain appears to expand toward the gallbladder region in the *Sox17*$^{+/-}$ embryos (also note *Sox4* expression in intrahepatic ductal plates of both two genotypes). **(B, C)** The qPCR analyses show the expression levels of *Sox4* and *Sox9* in wild-type and *Sox17*$^{+/-}$ gallbladders (**p<0.01). The *Sox4* expression level appears to be increased in the *Sox17*$^{+/-}$ gallbladders (p=0.077, B). Spearman rank correlation analysis of the association of these qPCR data (C) shows a significant correlation between these two genes in the wild-type and *Sox17*$^{+/-}$ gallbladders. dp, ductal plate; pv, portal vein. Scale bar: 50μm.

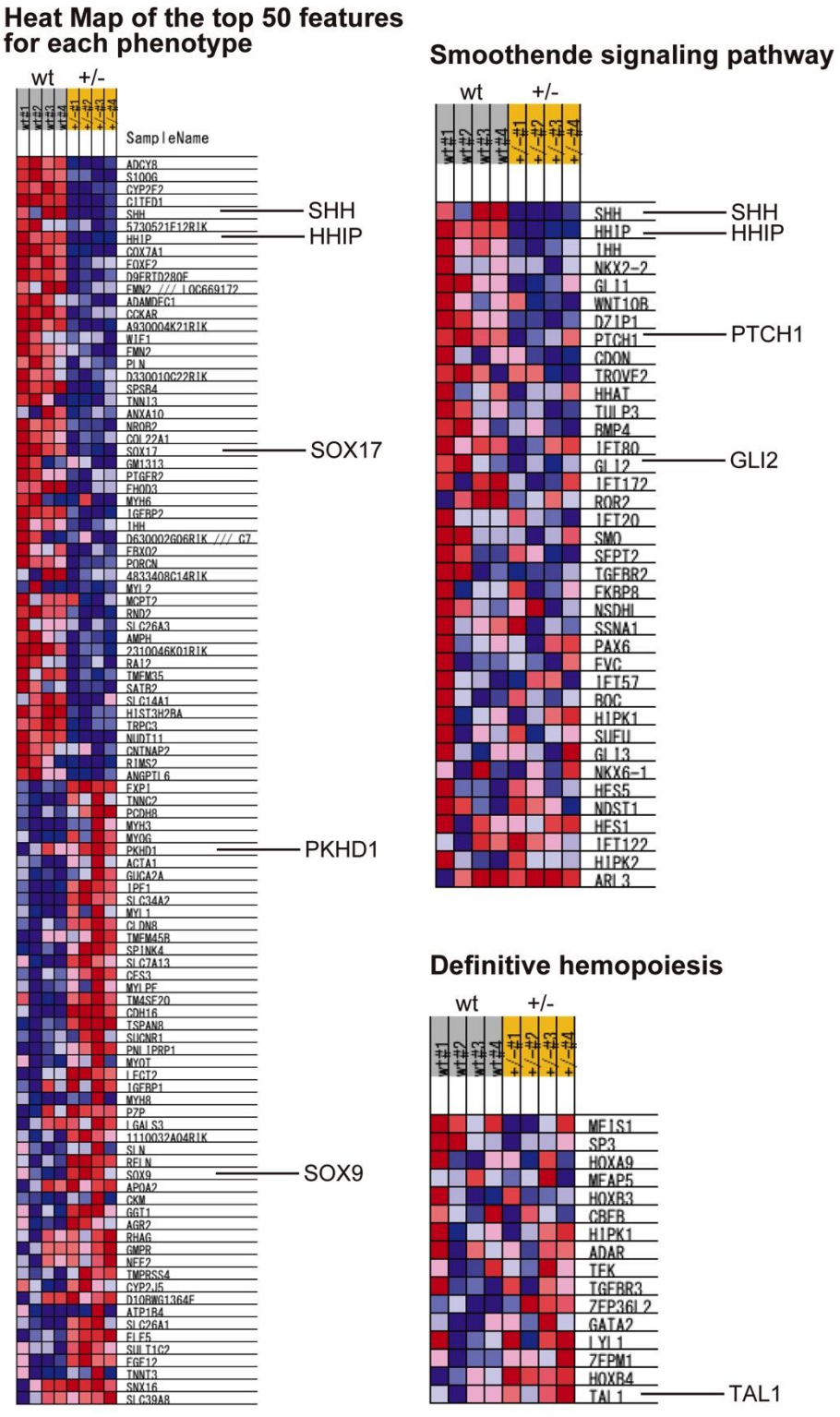

Fig. S4. Gene Set Enrichment Analysis (GSEA) analysis in wild-type and *Sox17*$^{+/-}$ gallbladders
The heat-map image of GSEA analysis shows enrichment of *Sox17* and *Sox9* as down- and up-regulated genes in the *Sox17*$^{+/-}$ gallbladders. *Shh* and its downstream genes (e.g., *Hhip*) are selected as shown in the result of "Smoothende_signaling_pathway", while the myeloid cell marker genes (e.g., *Tal1*) are enriched as "Definitive_hemopoiesis".

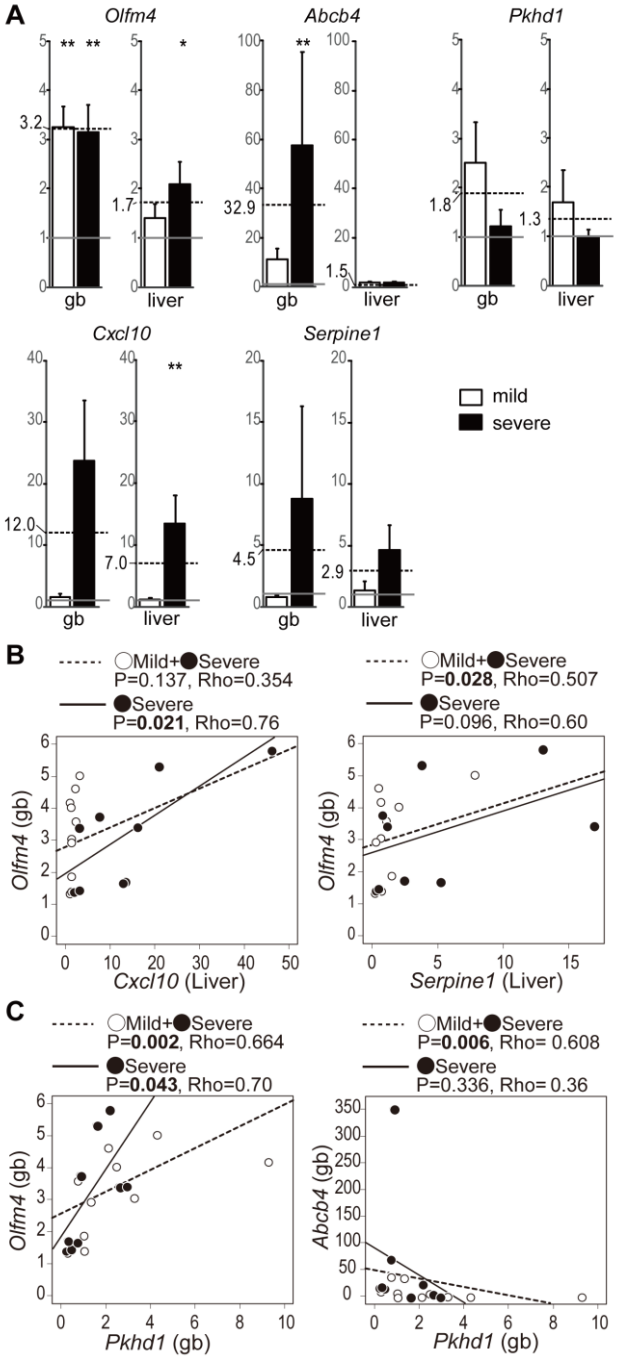

Fig. S5. Spearman rank correlation analysis of the association between the mRNA expression level of each marker gene in the gallbladder and liver of the *Sox17*$^{+/-}$ embryos at 17.5 dpc

(A) The fold change in the five genes (also see Figure 2C, D) in the *Sox17*$^{+/-}$ gallbladder (gb) and liver relative to the wild-type, in the mild and severe liver phenotypes. The expression levels of the wild-type are defined as 1 (gray horizontal lines) and the mean values of the levels of all *Sox17*$^{+/-}$ samples (i.e., mild + severe) are indicated by the dotted horizontal lines. *Olfm4* is significantly up-regulated in the *Sox17*$^{+/-}$ gallbladder both in the mild and severe samples, while *Abcb4* is significantly up-regulated only in the severe samples (*p<0.05, **p<0.01). **(B)** *Olfm4* mRNA levels in the gallbladder (y-axis) show a significant positive correlation with the expression levels of *Cxcl10* (the severe phenotype samples only) and *Serphine1* (all samples only) in the liver (hepatic inflammation markers; x-axis). **(C)** In the *Sox17*$^{+/-}$ gallbladders, *Pkhd1* (which encodes the ciliary protein fibrocystin) levels (x-axis) show a positive correlation with *Olfm4* mRNA levels in both the severe phenotype and all samples (y-axis), in contrast to its significant negative correlation with *Abcb4* mRNA levels in all samples (y-axis). Each solid (severe phenotype) and open (mild phenotype) circle indicates samples from each embryo with and without gross-anatomical hepatic lesions, respectively.

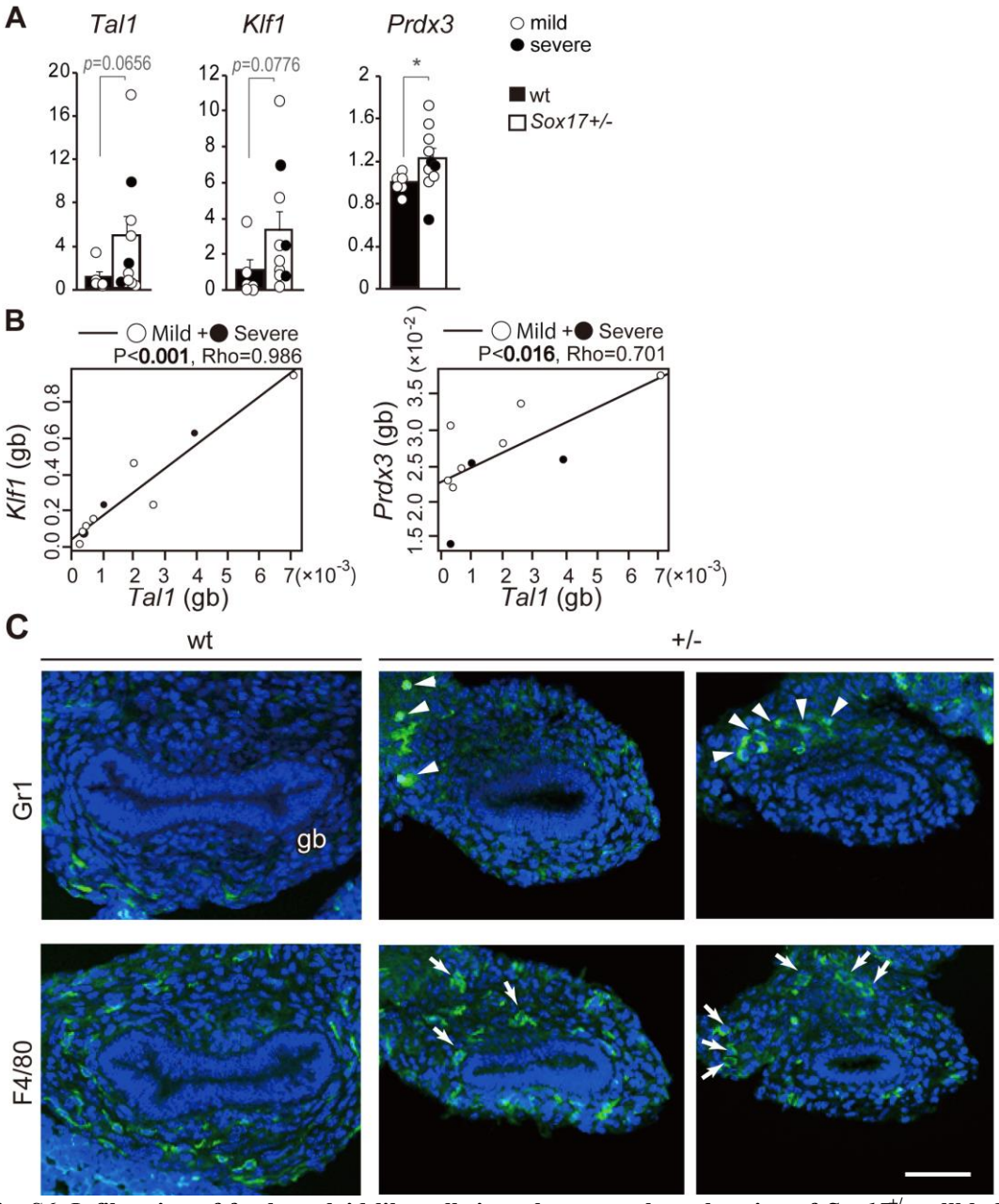

Fig. S6. Infiltration of fetal myeloid-like cells into the mesenchymal region of *Sox17*$^{+/-}$ gallbladders at 17.5 dpc *in vivo*

(A) The qPCR analyses of wild-type and *Sox17*$^{+/-}$ gallbladders at 17.5 dpc, showing the expression levels of three fetal myeloid cell markers (*Tal1, Klf1* and *Prdx3*) that are selected in the GO term 'myeloid cell differentiation' (see Figure 2). Each solid (severe phenotype) or open (mild phenotype) circle indicates the gallbladder sample from each embryo with or without gross-anatomical hepatic lesions, respectively. Despite hepatic lesions, all of these three markers show the tendencies of increased expression in *Sox17*$^{+/-}$ gallbladders (**p*<0.05). **(B)** Spearman rank correlation analysis showing that *Tal1* mRNA levels (x-axis) have a significant positive correlation with the expression levels of *Klf1* and *Prdx3* in the *Sox17*$^{+/-}$ gallbladders. **(C)** Immunofluorescence images (green) using anti-Gr1 (lymphocyte antigen 6 complex, locus G; Ly-6G) and anti-F4/80 (adhesion G protein-coupled receptor E1, Adgre1) antibodies, two fetal myeloid cell markers. Both Gr1-positive cells (arrowheads) and F4/80-positive large spherical cells (arrows) are frequently found in the surrounding mesenchyme, especially in the region facing to the fetal liver parenchyma in the *Sox17*$^{+/-}$ embryos. In contrast, the F4/80-positive small reticular cells with long and slender cytoplasmic processes are seen throughout the surrounding mesenchyme of both wild-type and *Sox17*$^{+/-}$ gallbladders (note the absence of either Gr1- or F4/80-positive cells within the epithelial layers of the *Sox17*$^{+/-}$ gallbladder). Scale bar: 50 μm.

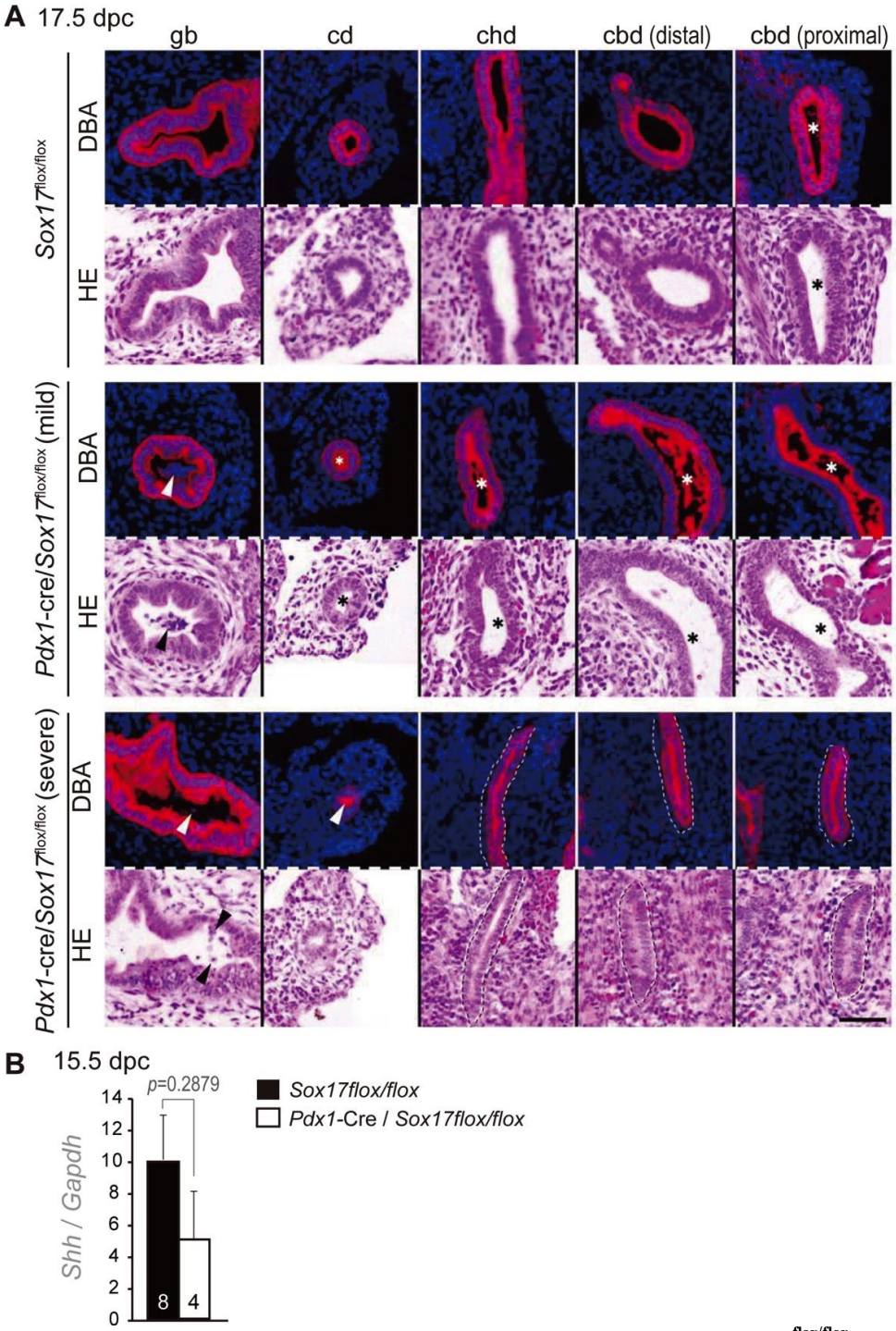

Fig. S7. Biliary atresia-like phenotypes in the biliary tract of *Pdx1*-cre/*Sox17*$^{flox/flox}$ embryos
(A) The DBA and HE staining images of the serial sections at the levels of gallbladder (gb), cystic duct (cd), common hepatic duct (chd) and common bile duct (cb) of the *Sox17*$^{flox/flox}$ (normal) and *Pdx1*-cre/*Sox17*$^{flox/flox}$ embryos with or without gross-anatomical hepatic lesions (severe and mild phenotypes). The DBA-positive decidual cells (arrowhead) and their debris (asterisk) are frequently in the fetal gallbladder and extrahepatic bile ducts of *Pdx1*-cre/*Sox17*$^{flox/flox}$ embryos. In the severe case, common hepatic- and common bile ducts are completely closed. **(B)** The qPCR analysis of the 15.5-dpc *Sox17*$^{flox/flox}$ and *Pdx1*-cre/*Sox17*$^{flox/flox}$ gallbladders, showing that the expression levels of *Shh* appear to be down-regulated in *Pdx1*-cre/*Sox17*$^{flox/flox}$ embryos, albeit with no significant differences (possibly due to the sample variation of the shortening gallbladder/cystic duct). The number inside the bar indicates the sample number used. cbd, common bile duct; cd, cystic duct; chd, common hepatic duct. Scale bar: 100 μm.

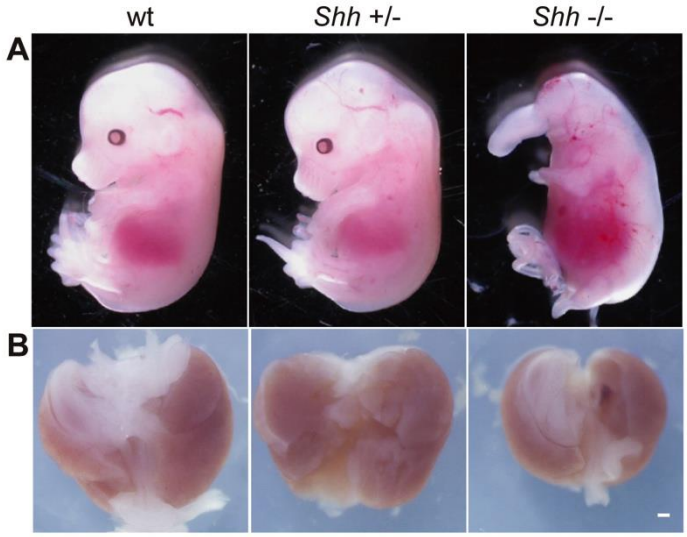

Fig. S8. Gross anatomical phenotypes of the livers of *Shh*-mutant embryos
(A, B) The external morphology of the whole embryo (wild-type, *Shh*$^{+/-}$ or *Shh*$^{-/-}$, **A**) and its liver attached to the digestive tract (caudal view, **B**) at 14.5 dpc. The *Shh*$^{-/-}$ embryo showed not only severe malformation of the head and limbs (**A**) but also growth retardation of the liver. Scale bar: 100 µm.

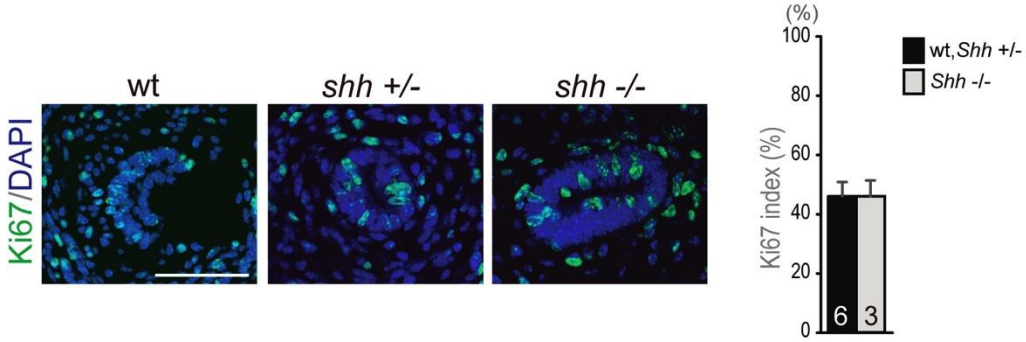

Fig. S9. Ki67-positive indices in the gallbladder primordia of wild-type, *Shh*$^{+/-}$ and *Shh*$^{-/-}$ embryos
The anti-Ki67 staining images of the transverse sections of the gallbladder region in the wild-type, *Shh*$^{+/-}$ and *Shh*$^{-/-}$ embryos at 14.5 dpc. The quantitative data of the Ki67-positive index shows the same levels between the *Shh*$^{-/-}$ and normal (*Shh*$^{+/-}$ and wildtype) samples. Scale bar: 100 µm.

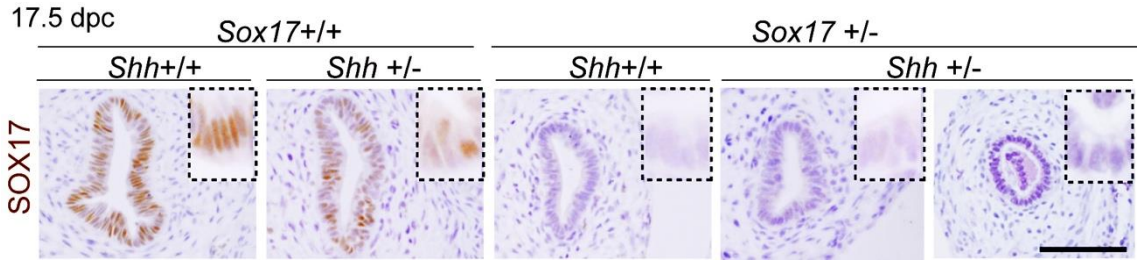

Fig. S10. The anti-SOX17 staining in transverse sections of fetal gallbladders of wild-type, *Shh*$^{+/-}$, *Sox17*$^{+/-}$ and *Sox17*$^{+/-}$/*Shh*$^{+/-}$ embryos at 17.5 dpc
The SOX17-positive signals in the gallbladder epithelia are not affected by the loss of the *Shh* allele. Also see figure 5D. Scale bar: 100 μm

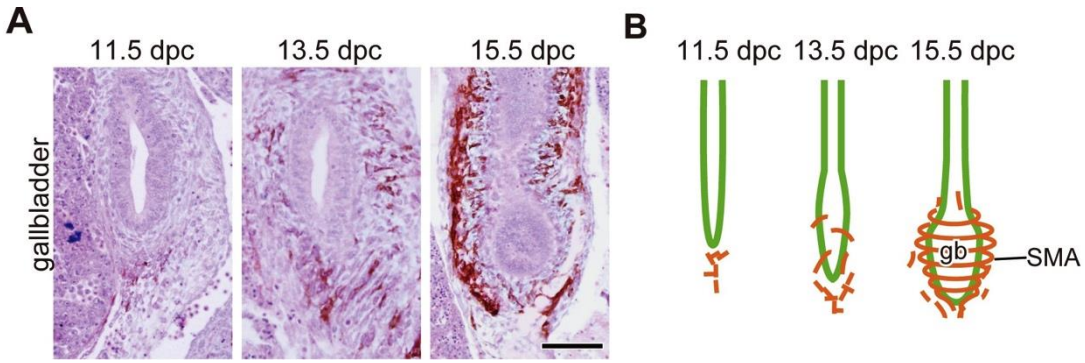

Fig. S11. Developmental patterns of the smooth muscle layers of the developing gallbladder in wild-type embryos
(A, B) The sagittal sectioning images of anti-SMA staining (brown color; **A**) and their schematic representation (**B**) of the developing mouse gallbladder during the early-to-late-organogenesis stages. At 11.5 dpc, SMA-positive cells first appear in the mesenchymal region at the distal tip of the primordial gallbladder. Patches of SMA-positive cells appear and expand to cover the gallbladder region beginning at 13.5 dpc. They ultimately form layers of smooth muscle around the organ at 15.5 dpc. Scale bar: 100 μm.

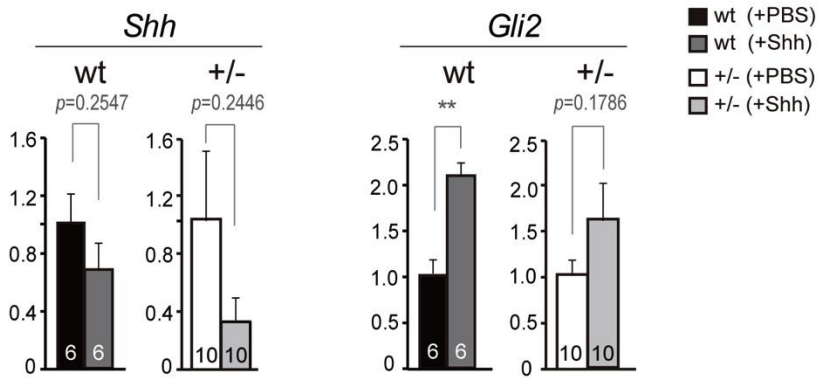

Fig. S12. Estimation of the cellular responses of exogenous Shh bead on the gallbladder explants *in vitro*
In the 3-day culture of the 13.5-dpc gallbladder explants, the addition of Shh bead weakly-to-moderately down- and up-regulates endogenous expression levels of *Shh* and *Gli2*, respectively (the mean value in each control PBS group is set as 1.0). The number inside the bar indicates the sample number used (see figure 7).

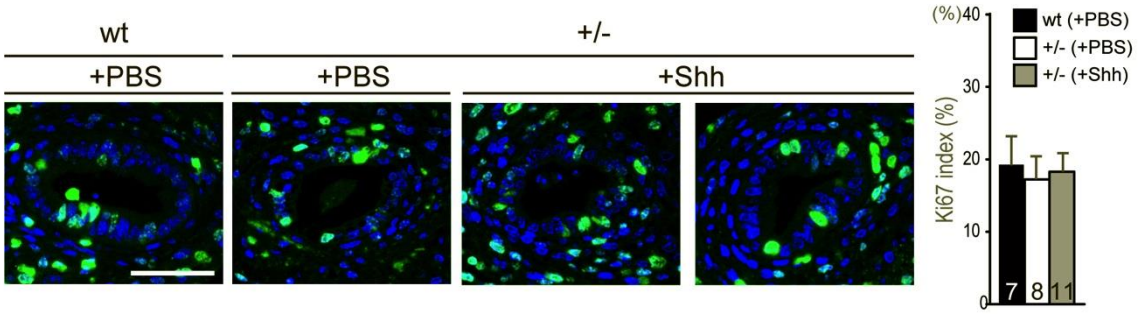

Fig. S13. Ki67-positive indices in the wild-type and *Sox17*$^{+/-}$ gallbladder explants with or without Shh beads *in vitro*

The anti-Ki67 staining (green fluorescence; transverse sections) of the 13.5-dpc wild-type and *Sox17*$^{+/-}$ gallbladder explants with or without Shh bead (3-day culture; see figure 7). The bar graph of the quantitative data of the Ki67-positive index shows no appreciable differences among three groups. Scale bar: 100 µm.

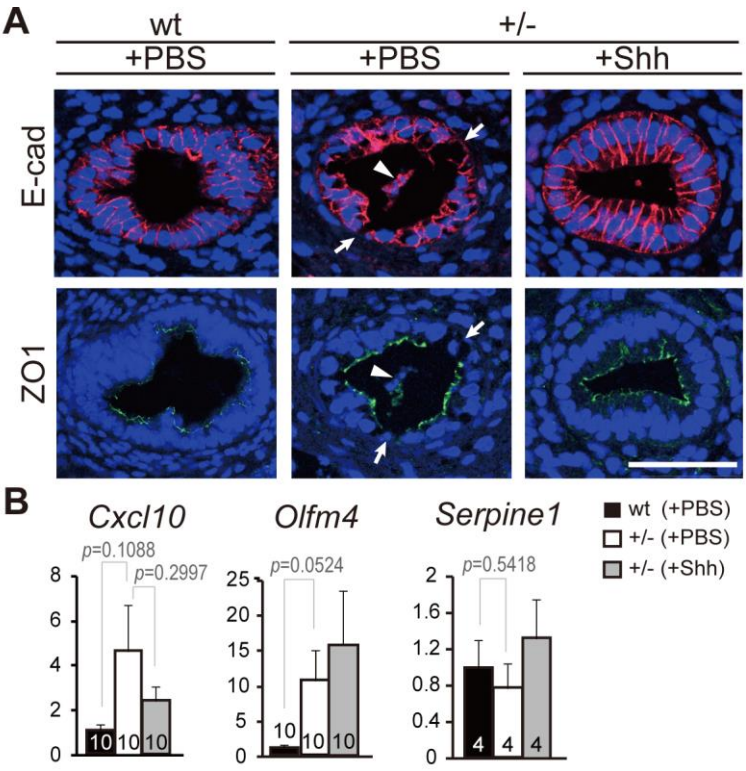

Fig. S14. Subcellular localization of apical and basal polarity markers and mRNA expression levels of early inflammatory (injury) markers in the wildtype and *Sox17*$^{+/-}$ gallbladder explants with or without Shh bead *in vitro*

(A) Anti-E-Cadherin (red) and anti-ZO1 (green) immunostaining of the wildtype and *Sox17*$^{+/-}$ gallbladder explants with or without Shh bead, showing proper subcellular localization of basolateral and apical surface domains even in the gallbladder epithelial cells near the injured site (note luminal decidual cells [arrowheads] and injured sites [arrows]). **(B)** The qPCR analysis of the wildtype and *Sox17*$^{+/-}$ gallbladder explants with or without Shh bead, showing a tendency to increased expression levels of *Cxcl10* and *Olfm4*, albeit not *Serpine1*, in the *Sox17*$^{+/-}$ explants as compared with the wild-type explants, but such increased expression of, at least, *Olfm4* could not be rescued by Shh-soaked bead. Scale bar: 50 µm.

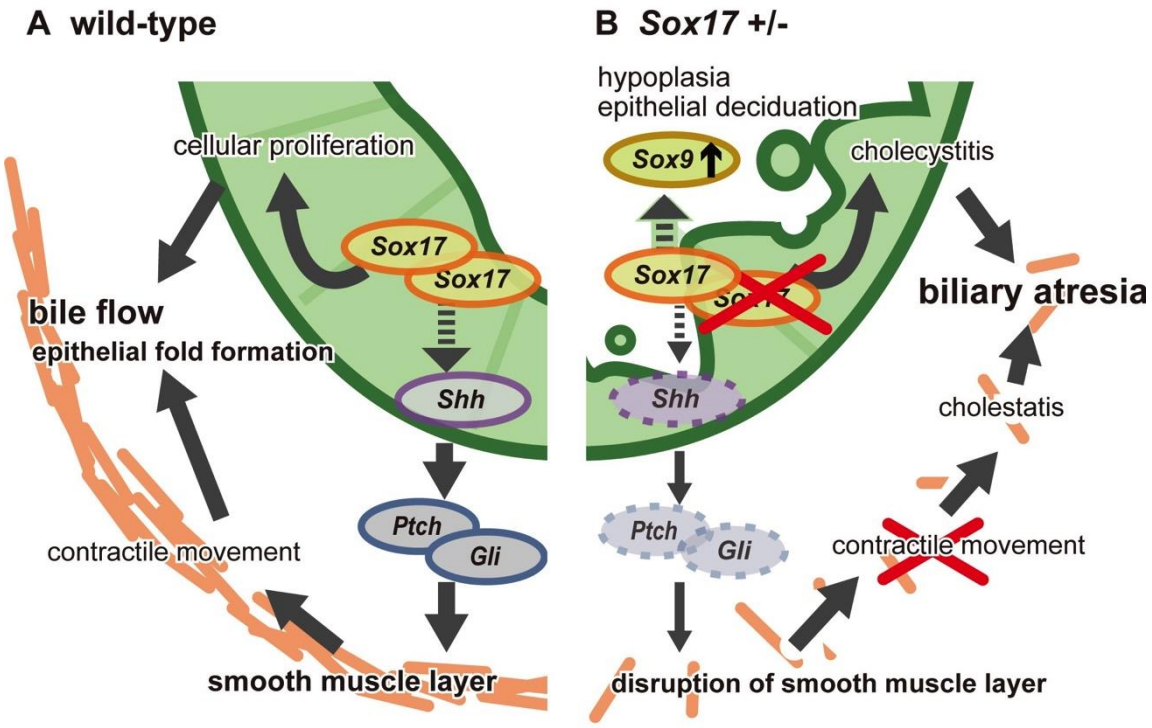

Fig. S15. Model for the pathogenesis of biliary atresia caused by *Sox17* haploinsufficiency
(**A**) In normal development, *Sox17* is expressed in the distal region of the gallbladder primordium, which is essential for the proliferation and maintenance of the gallbladder epithelium. The gallbladder epithelial cells express *Shh*, leading to the formation of contractile layers of circular smooth muscle, possibly through the actions of *Ptch* and *Gli* in the surrounding mesenchyme. (**B**) In the *Sox17*$^{+/-}$ gallbladder, gallbladder epithelium is replaced with SOX9-positive cystic duct-like epithelia, which may contribute partially to the onset of cholecystitis, as well as the hypoplasia and deciduation of gallbladder epithelia (i.e., luminal sloughed cells/cell debris) (Uemura et al. 2013). The reduced *Shh* expression in the *Sox17*$^{+/-}$ gallbladder severely affects the proper formation of smooth muscle layers surrounding the gallbladder epithelia, which consequently results in defective gallbladder contraction and cholestasis in the *Sox17*$^{+/-}$ embryos. Defective gallbladder contraction may cause a poor flow of bile fluid, leading to biliary atresia as a result of the luminal sloughed cells/cell debris.

Table S1. The up- and down regulated gene lists of the transcriptome analysis in *Sox17*$^{+/-}$ gallbladder compared with wild-type littermates at 15.5 dpc
This file contains the below list in each tab: 207 down-regulated genes in the *Sox17*$^{+/-}$ gallbladder which are also lower in the cystic duct than the gallbladder in the wild-type, 279 down-regulated genes in the *Sox17*$^{+/-}$ gallbladder, 221 up-regulated genes in the *Sox17*$^{+/-}$ gallbladder which are also higher in the cystic duct than the gallbladder, and 501 Up-regulated genes in the *Sox17*$^{+/-}$ gallbladder. Also see Figure 2.

Click here to Download Table S1

Supplemental Movie 1. Contractile movement of the wild-type gallbladder at 17.5 dpc
Time-lapse imaging (5 min, fast forwarding ×30 in timescale) of the wild-type gallbladder was conducted in pre-warmed 10% fetal calf serum-DMEM.

Supplemental Movie 2. Contractile movement of the *Sox17*$^{+/-}$ gallbladder at 17.5 dpc
Time-lapse imaging (5 min, forwarding ×30 in timescale) of the *Sox17*$^{+/-}$ gallbladder under the same conditions as in Supplementary Movie 1.

MATERIALS AND METHODS

Histology, lectin histochemistry, immunohistochemistry, and whole-mount *in situ* hybridization

For section immunohistochemistry, the sections or whole-mount samples were incubated in primary antibody: mouse anti-SMA (1/500 dilution; Sigma, A2547), rabbit anti-SOX9 (1/250 dilution; see Kidokoro et al., 2005), goat anti-SOX17 (1/200 dilution; R&D systems, AF1924), rabbit anti-E-cadherin (1/200 dilution; Cell Signaling Technology, 3195), mouse anti-ZO1 (1/100 dilution; Invitrogen, 33-9100), rat anti-Gr1 (1/500 dilution; BioLegend, 108403), and rat anti-F4/80 (1/100 dilution; BMA Biomedicals, T2008) in Tris-buffered blocking solution (TNB) for 12 h at 4°C. The secondary antibody was horseradish peroxidase (HRP)-conjugated goat anti-mouse IgG (Zymed Laboratories, San Francisco, CA, USA), biotin-conjugated secondary antibody in combination with an ABC Kit (Vector Laboratories), or secondary antibodies conjugated with Alexa-488/594 for light or fluorescence microscopy. They were diluted 1/400 in TNB and incubated 2 h at room temperature.

For whole-mount immunohistochemistry, samples were incubated in primary antibody (diluted 1/500 in TNB) for 2 days at room temperature, washed with PBS-T for 1 day, and incubated in secondary antibody (diluted 1/500 in TNB) for 2 days. For DBA lectin staining, the samples were incubated with Rhodamine-labeled DBA lectin (10 µg/mL) for 12 h at 4°C.

For fluorescent observation, the samples were counterstained with DAPI, and observed under an Olympus fluorescent microscope (BX51N-34-FL2), stereomicroscope (SZX16 plus U-LH100HG) systems, and the Leica TCS SP8 confocal laser microscope (Leica Microsystems GmbH). For whole-mount anti-SMA-stained samples, 1µm thick z-stack images were acquired by the confocal laser microscope, and 10 images were combined to obtain the 3D images.

Whole-mount *in situ* hybridization was performed as described by Hiramatsu et al. (2009). RNA probes targeting *Sox17* (Kanai et al., 1996), *Shh*, *Ihh* (Echelard et al., 1993), *Ptch* (Motoyama et al., 1998), *Gli1* (Liu et al., 1998), and *Sox4* (MGC, Clone ID: 5708894) were used for the present study. The stained samples were cryosectioned serially (7–15 µm in thickness).

RNA extraction, microarray, and qPCR analyses

The *Sox17*$^{+/-}$ and wild-type gallbladders at 15.5 dpc were used for microarray expression analysis according to the method developed by Huang et al. (2007, 2009). The sample number was 50 from each genotype, and the ratio of male to female was 1:1. The total RNA from all samples was purified using the QIAGEN RNeasy Micro Kit according to the protocols in the GeneChip 3' IVT Express kit (Affymetrix). Fragmented RNA was hybridized to mouse genome 430 2.0 arrays (Affymetrix), and chips were washed and stained using the Fluidics Station 450 (Affymetrix). The arrays were scanned using the GeneChip scanner 3000 (Affymetrix), and the output was collected by GeneChip Operating Software or Expression Console (Affymetrix). Data were normalized and further analyzed by the RMA method using AltAnalyze software (Emig et al., 2010; http://www.altanalyze.org/). On unsupervised clustering, DAVID was used (http://david.abcc.ncifcrf.gov/). The microarray data have been deposited in the Gene Expression Omnibus of NCBI (accession number: GSE 74576).

The Gene Set Enrichment Analysis (GSEA) was carried out using the methods of Subramanian et al. (2005) as implemented in the software provided by the Broad Institute (http://www.broad.mit.edu/gsea/).

For qPCR analysis, total RNA was reverse-transcribed using random primers and the Superscript-III cDNA synthesis kit (Invitrogen). Specific primers and fluorogenic probes for *Sox17* (Mm00488363_m1), *Shh* (Mm00436528_m1), *Gli1* (Mm00494645_m1), *Gli2* (Mm01293111_m1), *Gli3* (Mm00492345_m1), *Hhip* (Mm00469580_m1), *Sox9* (Mm00448840_m1), *Sox4* (Mm00486320_m1), *Abcb4* (Mm00435630_m1), *Olfm4* (Mm01320260_m1), *Pkhd1* (Mm00467739_m1), *Cxcl10* (Mm00445235_m1), *Serpine* (Mm00435860), *Tal1* (Mm01187033_m1), *Klf1* (Mm00516096_m1), *Prdx3* (Mm00545848_m1), and *Gapdh* (Taqman control reagents) were purchased from Applied Biosystems. PCR was performed using the Applied Biosystems Step One Real Time PCR System. The expression levels are presented as the expression levels of each marker gene relative to *Gapdh* expression (mean ± standard error).